Electronic Supplementary Material (ESI) for Nanoscale.

On the Photophysics of Nanographene – Investigation of functionalized Hexa-peri-hexabenzocoronenes as Model Systems

Philipp Haines, David Reger, Johannes Träg, Volker Strauss, Dominik Lungerich, Dirk Zahn, Norbert Jux, Dirk M. Guldi

Abstract: In the current study, we report on hexa-peri-hexabenzocoronenes (HBCs) as a representative model for nanographene. To this end, we synthesized a family of functionalized HBCs and investigated the impact of the substituents on the π-extended system of the HBCs. DFT and TD-DFT calculations suggested a charge transfer character, which intensifies as the electron density withdrawing effects of the substituents (–M-effect) increase. Unambiguous corroboration of the charge transfer character in the case of the NO_2-substituents was realized with steady-state absorption and fluorescence experiments, which focused on the dependencies on solvent polarity and temperature featuring. Going beyond HBCs with NO_2-substituents time-correlated single photon counting, femtosecond and nanosecond transient absorption spectroscopy unveil long-lived singlet and triplet excited states. As a complement, we performed electrochemical and spectroelectrochemical measurements. These were carried out to shed light onto the nature of functionalized HBCs as electron acceptors and/or donors, on one hand, and their corresponding spectroscopic signatures, on the other hand. All of the aforementioned enabled intermolecular charge separation assays with, for example, suitable electron acceptors by steady-state and time-resolved spectroscopies.

Table of Contents

Experimental Procedures

All chemicals were purchased from Sigma-Aldrich and used without any further purification. Steady-state absorption experiments were performed using a Lambda 2 spectrophotometer from Perkin Elmer. The measurements were conducted in a 10mm×10mm quartz cuvette. Steady state fluorescence measurements were also carried out in a 10mm×10mm quartz cuvette. The instrument was a FluoroMax®-3 fluorometer from Horiba Jovin Yvon equipped with a R928P photomultiplier tube from Hamamatsu (185 –850 nm). Temperature-dependent emission measurements were performed using an OptistatDN2 cryostat from Oxford. Time correlated single-photon counting (TCSPC) experiments were recorded with a FluoroLog®-3 lifetime spectro-fluorometer from Horiba Jobin Yvon with integrated TCSPC software. The samples were excited at 400 nm by a SuperK Extreme EXB-6 laser from NKT Photonics. The signal was detected by a Hamamatsu MCP photomultiplier (R33809U-50). All measurements were performed using a 10mm×10mm quartz cuvette. Femtosecond transient absorption spectroscopy measurements were performed using transient absorption pump/probe system EOS from Ultrafast Systems. Laser pulses were generated with an amplified titanium:sapphire CPA-2110 fs laser system (775 nm output, 1 kHz repetition rate, 150 fs pulse width; 200 nJ excitation laser energy) from Clark-MXR Inc. The desired excitation at 387 nm was tuned by frequency doubling using a calcium fluoride non-linear optical crystal. The spectral width is detected from 400 to 915 nm by two CCD cameras. The measurements were carried out using a 2 mm quartz cuvette. The transient absorption spectra were recorded with the software EOS from Newport/Ultrafast Systems. Electrochemical measurements were carried out with a three-electrode setup. A glassy carbon disk served as working electrode, an Ag/AgCl was used as reference electrode and a Pt-plate was used as counter electrode. Voltage was controlled with an EG&G Princeton Applied Research potentiostat. The data was recorded with NOVA 1.10 software. Spectro-electrochemistry was conducted with a home-made three neck cell in a Cary 5000 UV/Vis/NIR spectrometer from Varian and the respective processing software. We used a three-electrode setup consisting of a Pt-gauze as working electrode, a Pt-wire as counter electrode and a silver wire as pseudo reference electrode.

Synthesis

General Information

All chemicals were purchased from Sigma-Aldrich and used without any further purification. Solvents were distilled prior to usage. CH_2Cl_2, $CHCl_3$ and EtOAc were distilled from K_2CO_3 prior to usage. Thin layer chromatography (TLC) was performed on Merck silica gel 60 F254, detected by UV-light (254 nm, 366 nm). Column chromatography and flash column chromatography were performed on Macherey– Nagel silica gel 60 M (230–400 mesh, 0.04–0.063 mm). NMR spectroscopy was performed on JEOL JNM EX 400 (^{1}H: 400 MHz, ^{13}C: 100 MHz) and JEOL JNM GX 400 (^{1}H: 400 MHz, ^{13}C: 100 MHz) and Bruker Avance 400 (^{1}H: 400 MHz, ^{13}C: 100 MHz). Deuterated solvents were purchased from Sigma Aldrich and used as received. Chemical shifts are referenced to residual protic impurities in the solvents ($CHCl_3$: ^{1}H: 7.26 ppm) or the deuterated solvent itself ($CDCl_3$: ^{13}C; 77.0 ppm). The resonance multiplicities are indicated as “s“ (singlet), “d” (doublet), “t” (triplet), “q” (quartet) and “m” (multiplet). Signals referred to as bs (broad singlet) are not clearly resolved or significantly broadened. Para-substituted phenylrings with an AA’BB’ spin system are termed as multiplets. LDI/MALDI-ToF mass spectrometry was performed on a Shimazu AXIMA Confidence (nitrogen laser, 50 Hz, 337 nm) or on a Bruker ultraflexToF/ToF instrument (nitrogen laser, 50 Hz, 337 nm) .In case of MALDI, the following matrix were used: 2,5-dihydroxybenzoic acid (DHB), sinapic acid (SIN) or trans-2-[3-(4-tert-butylphenyl)-2-methyl-2-propenylidene]malononitrile (DCTB). High resolution mass spectrometry was performed on an ESI-ToF mass spectrometer Bruker maXis 4G UHR MS/MS spectrometer or a Bruker micrOTOF II focus TOF MS-spectrometer or via MALDI-ToF instrument Bruker ultraflexToF/ToF (nitrogen laser, 50 Hz, 337 nm).

Ethyl 4-((4-(tert-butyl)phenyl)ethynyl)benzoate (Ac-COOEt)

A round-bottom pressure flask (250 mL) equipped with a magnetic stirring bar was charged with ethyl 4-bromobenzoate (3.00 g, 2.14 mL, 13.1 mmol), $Pd(PPh_3)_2Cl_2$ (0.18 g, 0.26 mmol), CuI (24.7 mg, 0.13 mmol), diisopropylamine (40 mL) and THF (40 mL). The reaction mixture was degassed by bubbling N_2 through the solution for 15 min. Finally 4-*tert*-butylphenyl acetylene (2.18 g, 2.49 mL, 13.8 mmol) was added and the flask was closed. The reaction mixture was stirred over night for 15.5 h at 100 °C. After cooling to room temperature all solvents were evaporated and the crude, blackish product was purified via column chromatography over silica gel with hexanes/CH_2Cl_2 2/1. The product was obtained as a pale orange solid which was recrystallized from *n*-pentane (50 mL). Two subsequent crystallizations gave the off-white product in an overall yield of 81 % (3.21 g, 10.5 mmol).
^{1}H NMR ($CDCl_3$, 400 MHz, rt.): δ [ppm] = 8.04 – 8.01 (m, 2H, 11), 7.59 – 7.56 (m, 2H, 10), 7.50 – 7.47 (m, 2H, 4/5), 7.40 – 7.38 (m, 2H, 4/5), 4.39 (q, 2H, ^3J = 7.2 Hz, 14), 1.41 (t, 3H, ^3J = 7.2 Hz, 15), 1.33 (s, 9H, 1).
^{13}C NMR ($CDCl_3$, 100 MHz, rt.): δ [ppm] = 166.1 (13), 152.1 (3), 131.5 (10/11), 131.4 (10/11), 129.6 (6/9/12), 129.4 (4/5), 128.1 (6/9/12), 125.4 (4/5), 119.7 (6/9/12), 92.5 (7/8), 88.1 (7/8), 61.1 (14), 34.8 (2), 31.1 (1), 14.3 (15).

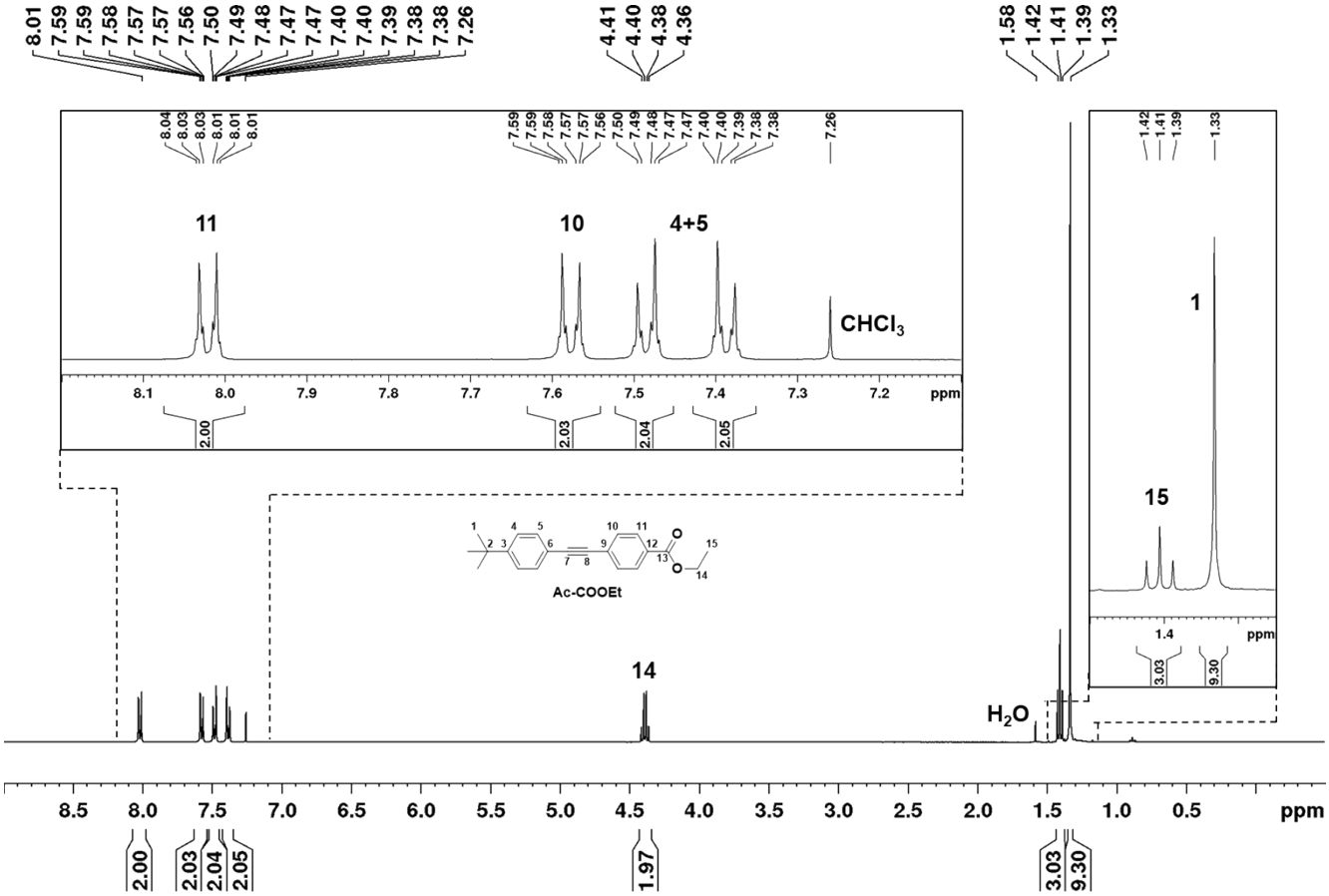

Figure S1: ^{1}H NMR spectrum of **Ac-COOEt** in $CDCl_3$ (400 MHz, rt.).

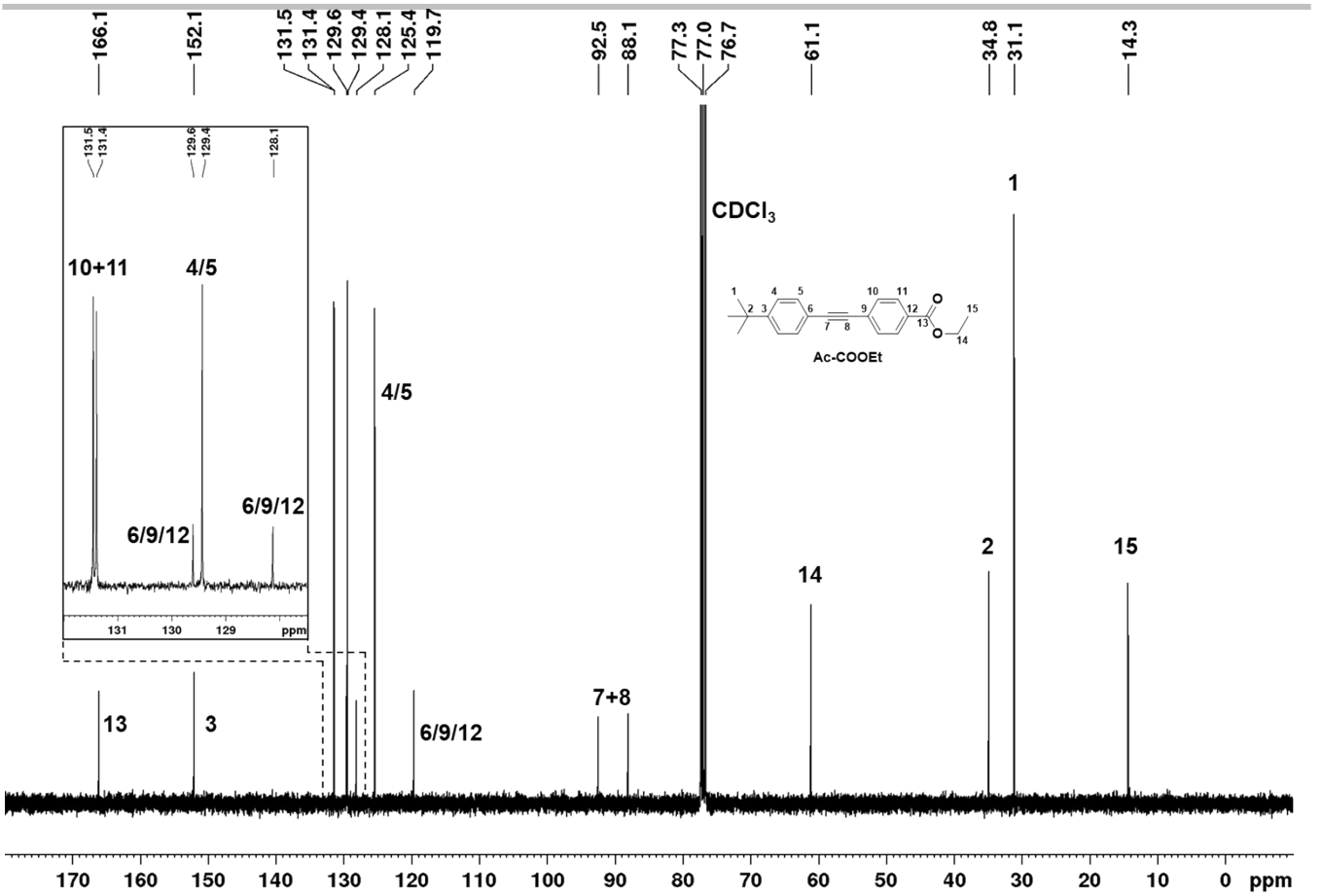

Figure S2. ^{13}C NMR spectrum of **Ac-COOEt** in $CDCl_3$ (100 MHz, rt.).

Pentakis-tert-butyl-mono-ethyl ester HAB (HAB-COOEt)

A round-bottom pressure-flask (100 mL) equipped with a magnetic stirring bar was charged with **Ac-COOEt** (0.25 g, 0.80 mmol), **TC** (0.49 g, 0.80 mmol) and toluene (4 mL). The flask was purged with N_2 and closed. The dark violet suspension was stirred for 26.5 h at 220 °C. After cooling to room temperature CH_2Cl_2 (5 mL) were added to dissolve everything. Methanol (25 mL) was added while stirring and a white solid precipitated immediately. The suspension was cooled in the fridge and then filtered through a glass frit (P4). The white solid was washed with an excess of methanol. A second precipitation under the same conditions yielded a second crop of product. The product was dried under vacuum and was obtained as a white solid with a yield of 90 % (0.64 g, 0.72 mmol).
^{1}H NMR ($CDCl_3$, 400 MHz, rt.): δ [ppm] = 7.55 – 7.53 (m, 2H, 1), 6.95 – 6.93 (m, 2H, 2), 6.83 – 6.79 (m, 10H, 3/4/5/6/7/8), 6.69 – 6.63 (m, 10H, 3/4/5/6/7/8), 4.25 (q, 2H, ^3J = 7.1 Hz, 12), 1.30 (t, 3H, ^3J = 7.1 Hz, 13), 1.10 (s, 18H, 9/10/11), 1.09 (s, 27H, 9/10/11).
^{13}C NMR ($CDCl_3$, 100 MHz, rt.): δ [ppm] = 166.9, 147.9, 147.53, 147.47, 146.4, 141.0, 140.7, 139.9, 138.8, 137.72, 137.65, 137.4, 131.6, 131.01, 130.97, 127.7, 126.8, 123.3, 123.1, 123.0, 60.5, 34.1, 34.04, 34.03, 31.2, 14.2.
MS (MALDI-ToF): No product peak detected.

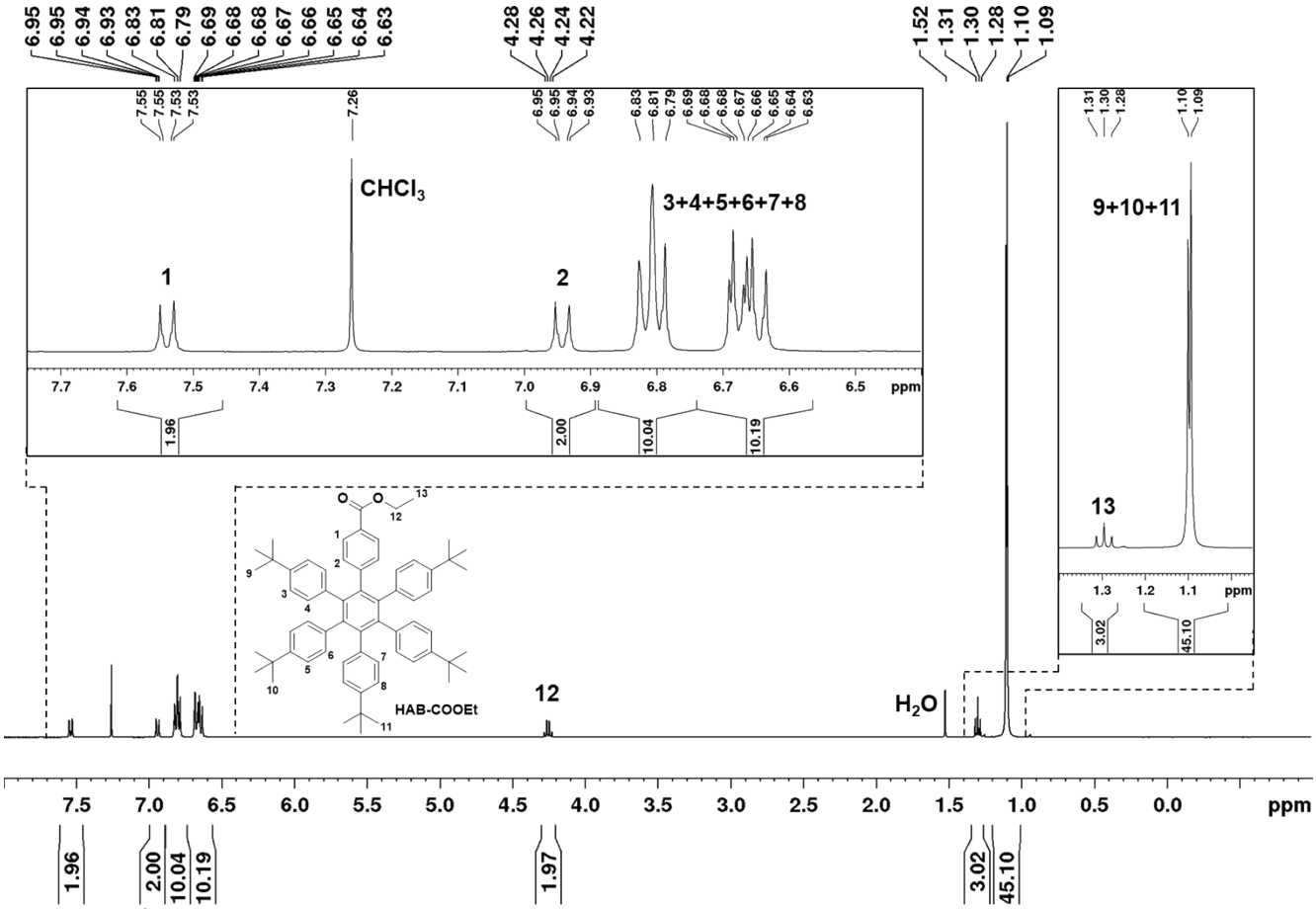

Figure S3. ^{1}H NMR spectrum of **HAB-COOEt** in $CDCl_3$ (400 MHz, rt.).

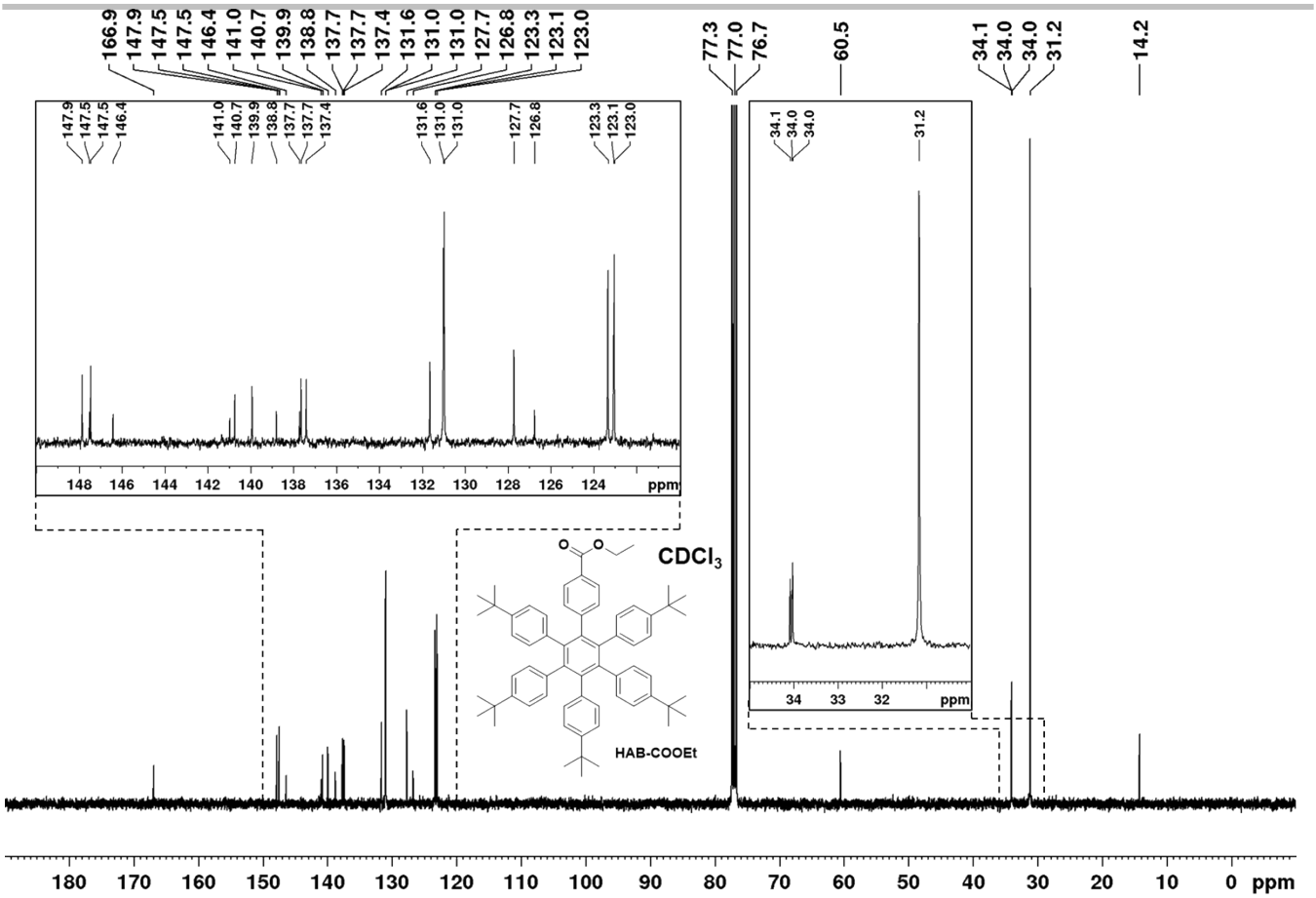

Figure S4. ^{13}C NMR spectrum of **HAB-COOEt** in $CDCl_3$ (100 MHz, rt.).

Pentakis-tert-butyl-mono-ethyl ester HBC (HBC-COOEt)

A round-bottom Schlenk flask (500 mL) equipped with a magnetic stirring bar and a septum was charged **HAB-COOEt** (0.30 g, 0.34 mmol) and CH_2Cl_2 (200 mL). The solution was degassed by N_2 bubbling for 20 min. Meanwhile the mixture was cooled to 0 °C in an ice-bath. $FeCl_3$ (0.88 g, 5.44 mmol) dissolved in $MeNO_2$ (3.00 mL) was added at 0 °C over 15 min. Meanwhile N_2 bubbling and cooling was continued. Cooling and N_2 stream was continued for further 45 min. The ice-bath was removed and the brownish reaction mixture was stirred under N_2 (no stream) for 20.5 h at room temperature. Methanol (150 mL) was added to give yellow solution. CH_2Cl_2 (approximately 100 mL) was removed by evaporation and a yellow solid precipitated. The suspension was cooled in the fridge for 1.5 h. The solid was filtered off through a glass frit (P4) and washed with an excess of methanol until the filtrate remained colourless. The solid was dried under vacuum and the product was obtained as a bright yellow powder with a yield of 90 % (267 mg, 0.31 mmol).

^{1}H NMR ($CDCl_3$, 400 MHz, rt.): δ [ppm] = 9.57 (s, 2H, 1), 9.19 (s, 2H, 2/3/4/5/6), 9.16 (s, 2H, 2/3/4/5/6), 9.13 (s, 2H, 2/3/4/5/6), 9.10 (s, 2H, 2/3/4/5/6), 9.07 (s, 2H, 2/3/4/5/6), 4.73 (q, 2H, ^3J = 7.1 Hz, 10), 1.85 (s, 9H, 9), 1.83 (s, 18H, 7/8), 1.79 (s, 18H, 7/8), 1.69 (t, 3H, ^3J = 7.1 Hz, 11).

^{13}C NMR ($CDCl_3$, 100 MHz, rt.): δ [ppm] = 167.5, 148.9, 148.8, 148.7, 130.5, 130.4, 130.2, 130.1, 130.0, 129.7, 128.2, 127.3, 123.45, 123.42, 122.1, 121.1, 120.9, 120.1, 119.3, 119.2, 119.0, 118.7, 61.5, 35.7, 32.1, 32.0, 14.7.

MS (MALDI-ToF, dhb): m/z = 874 $[M]^+$

HRMS (MALDI-ToF, dhb): m/z (calculated for $C_{65}H_{62}O_2$): 874.4744 $[M]^+$

m/z (measured): 874.474 $[M]^+$

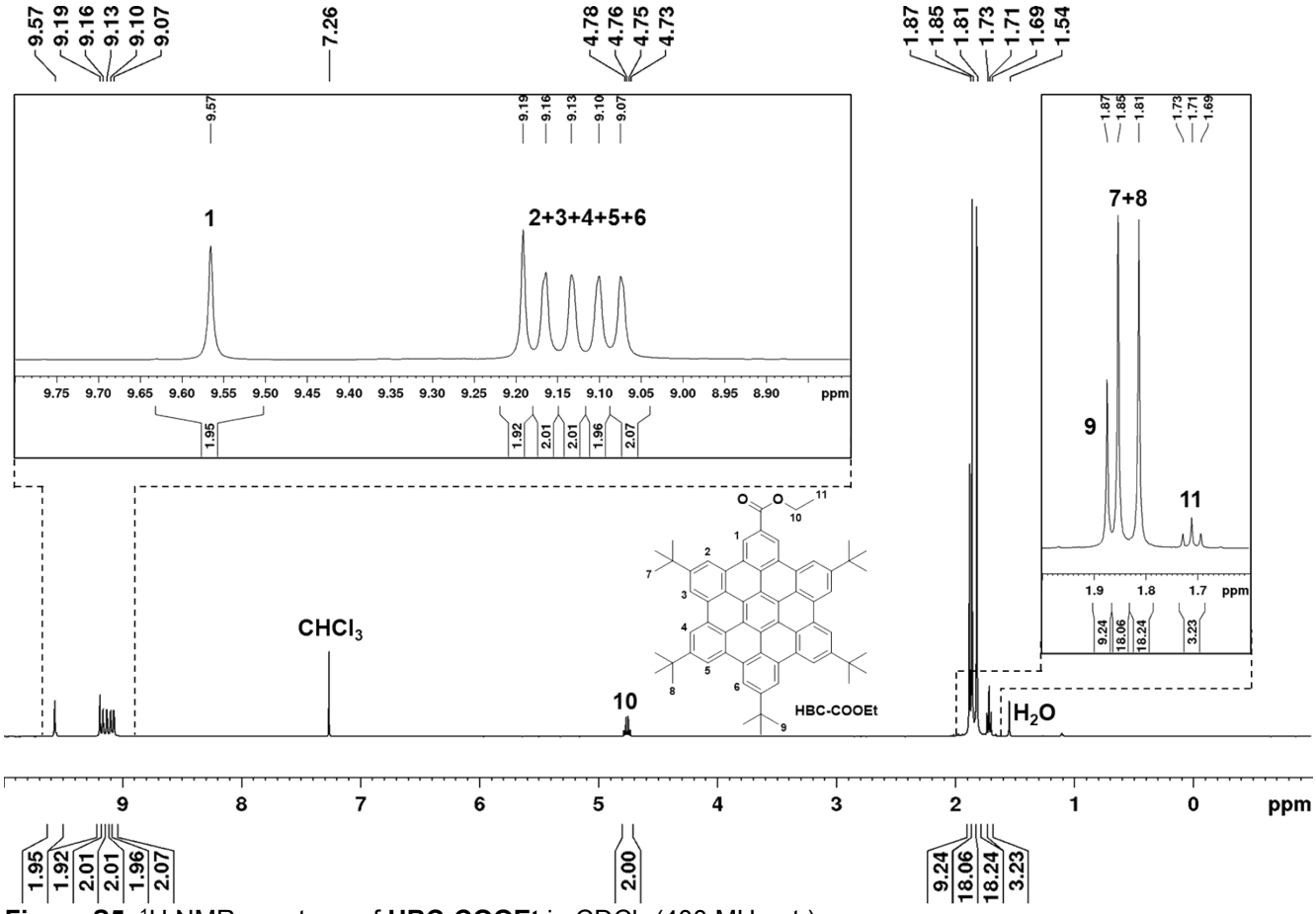

Figure S5. ^{1}H NMR spectrum of **HBC-COOEt** in $CDCl_3$ (400 MHz, rt.).

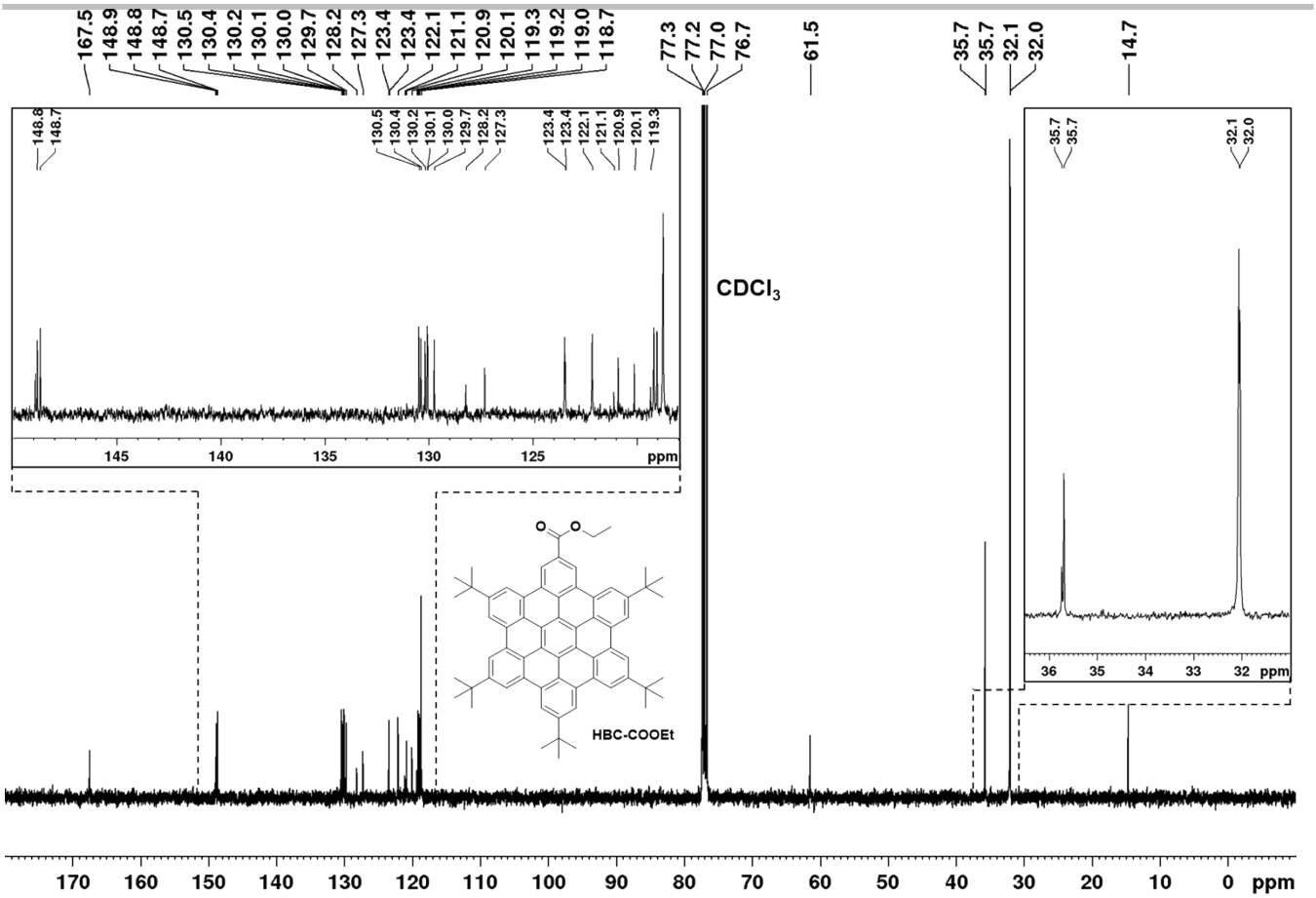

Figure S6. ^{13}C NMR spectrum of **HBC-COOEt** in $CDCl_3$ (100 MHz, rt.).

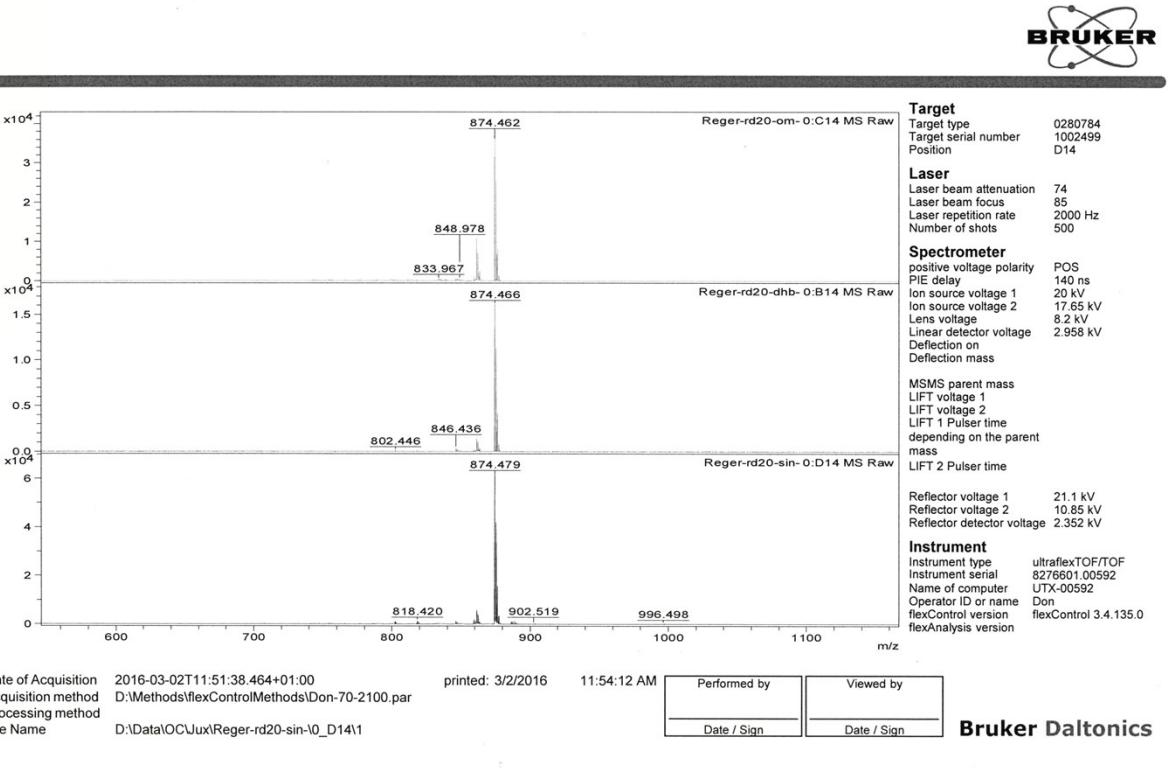

Figure S7. MALDI-ToF spectra of **HBC-COOEt** (top: without matrix; mid: dhb; bottom: sin).

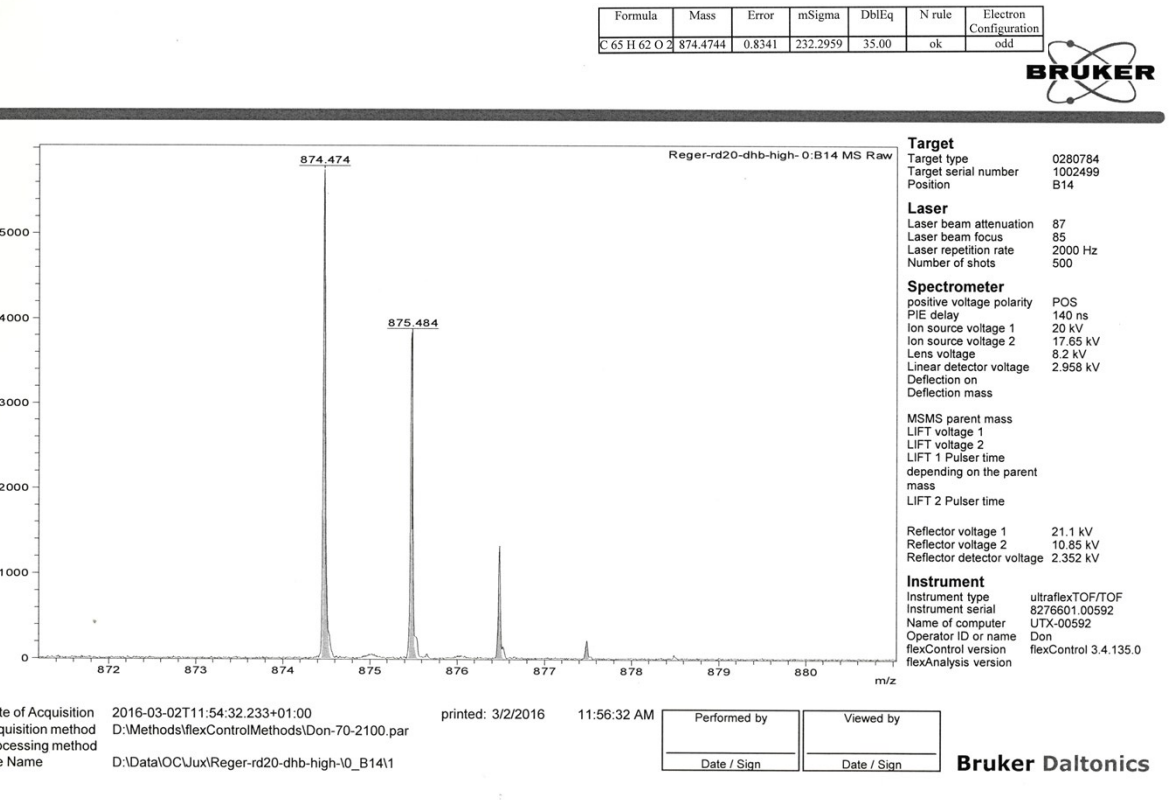

Figure S8. HRMS MALDI-ToF of **HBC-COOEt** (dhb). Simulated MS as grey background; inset: Calculated mass.

Pentakis-tert-butyl-mono-carboxylic acid HBC (3)

*Via saponification of **HBC-COOEt***

A pressure vial (20 mL) equipped with a magnetic stirring bar was charged with **HBC-COOEt** (0.13 g, 0.15 mmol) dissolved in THF (5 mL). 10 M aq. NaOH (1.2 g, 30.0 mmol in 3 mL H_2O) was added, the vial was closed and the reaction mixture was stirred for 68 h at 90 °C. During that time a yellow solid precipitated. The reaction mixture was poured onto 10 % aq. HCl (50 mL) and was stirred for 30 min. A small amount of MTBE was added and the phases were separated. The organic phase was washed with H_2O (3 x 50 mL) and all solvents were removed under reduced pressure. The remaining yellow solid was suspended in CH_2Cl_2 (20 mL) and methanol (20 mL) was added. The solid was filtered off and washed with an excess of methanol and CH_2Cl_2 until the filtrate remained colourless. The solid was dried under vacuum and the product was obtained as a dark yellow solid in a yield of 80 % (0.10 g, 0.12 mmol).
No suitable NMR could be measured due to the low solubility of the product.
MS (MALDI-ToF, dctb): m/z = 846 $[M]^+$
HRMS (MALDI-ToF, dctb): m/z (calculated for $C_{63}H_{58}O_2$): 846.4431 $[M]^+$
m/z (measured): 846.4445 $[M]^+$

*Via oxidation of **HBC-CHO***

A round-bottom flask (100 mL) equipped with a magnetic stirring bar was charged with **HBC-CHO** (72 mg, 87 µmol), dissolved in hot THF (50 mL) and 18crown6 (23 mg, 87 µmol) was added. The mixture was cooled to room temperature and a solution of $KMnO_4$ (26 mg, 165 µmol) in H_2O (6 mL) was added. The mixture was stirred for 72 h at room temperature. The solvent was removed and crude was purified by silica gel filtration (1. CH_2Cl_2, 2. THF, 3. THF/AcOH). Fraction three contained the yellow product in a yield of 29 % (21 mg ,25 µmol).
For the characterization see procedure above.

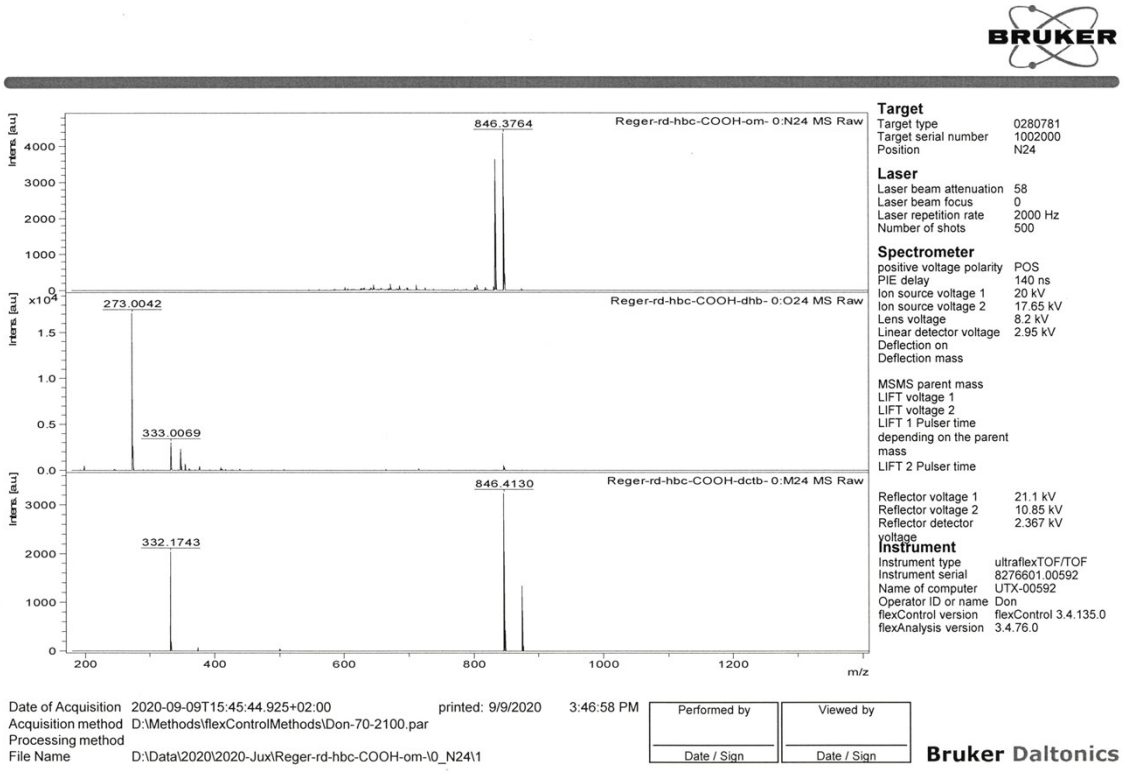

Figure S9. MALDI-ToF spectra of **3** (overview) (top: without matrix; mid: dhb; bottom: dctb). The peak at 874 which is mainly observed for dctb as the matrix corresponds to the precursor **HBC-COOEt**. However, as we never observed significant impurities with other measurements we assume that this is a minor impurity that is just easily ionized with dctb as the matrix and therefore observed.

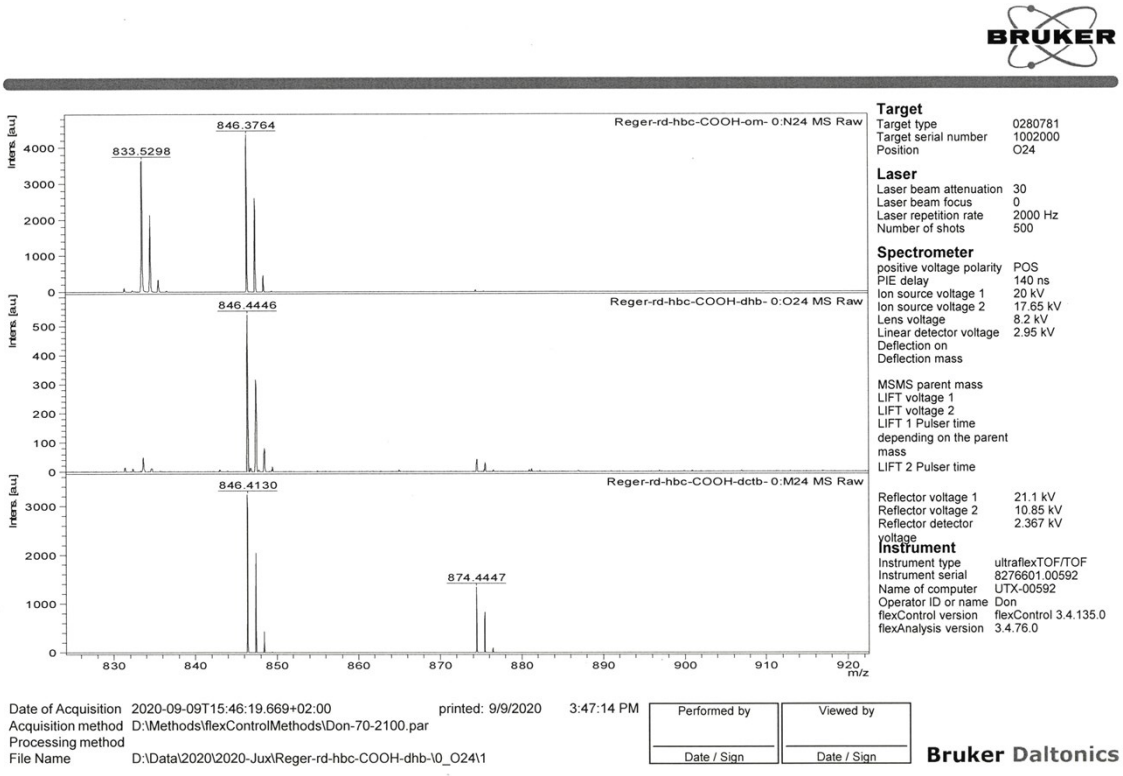

Figure S10: MALDI-ToF spectra of **3** (zoom on product peak) (top: without matrix; mid: dhb; bottom: dctb). The peak at 874 which is mainly observed for dctb as the matrix corresponds to the precursor **HBC-COOEt**. However, as we never observed significant impurities with other measurements we assume that this is a minor impurity that is just easily ionized with dctb as the matrix and therefore observed.

Formula	Mass	Error	mSigma	DblEq	N rule	Electron Configuration
C 63 H 58 O 2	846.4431	1.6285	53.6685	35.00	ok	odd

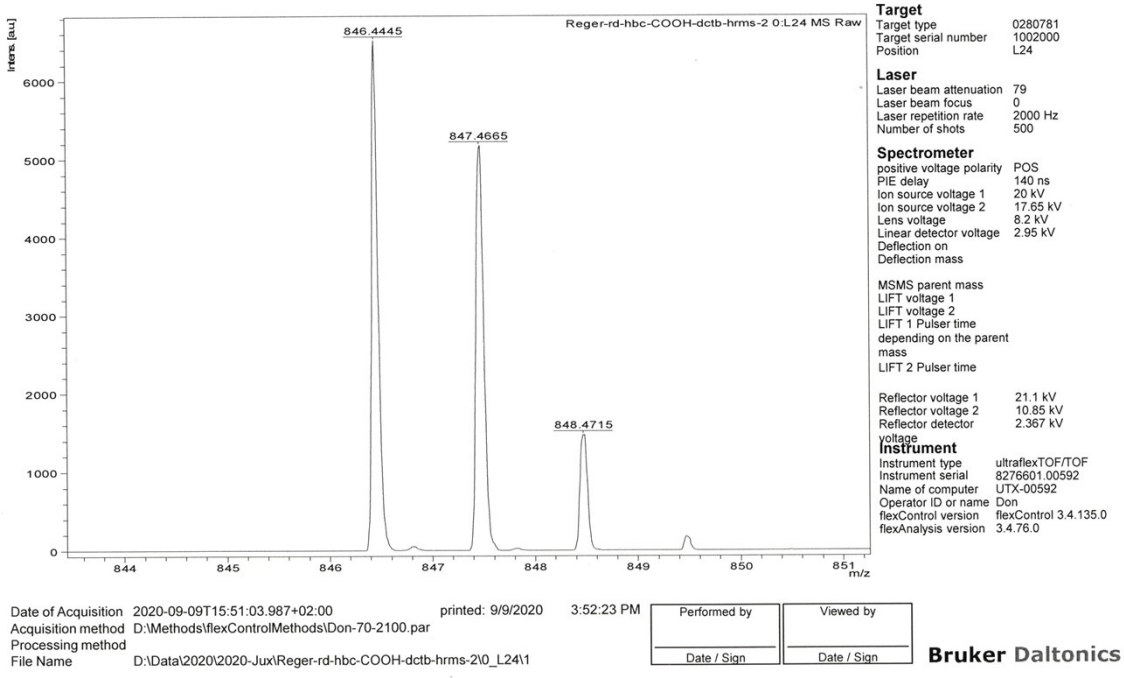

Figure S11. HRMS MALDI-ToF of **3** (dctb). Inset: Calculated mass.

Pentakis-tert-butyl-mono-n-butyl-carboxamid HBC (2)

A reaction vial (2 mL) equipped with a magnetic stirring bar was charged with **HBC-COOH** (50.0 mg, 59.0 µmol), 1-Hydroxybenzotriazol (HOBt) hydrate (16.2 mg, 0.12 mmol), 1-Ethyl-3-(3-dimethylaminopropyl)carbodiimid x HCl (23.0 mg, 0.12 mmol), CH_2Cl_2 (1.5 mL), N,N-diisopropylethylamine (23.3 mg, 30.7 µL, 0.18 mmol) and n-butylamine (8.78 mg, 11.9 µL, 0.12 mmol). The suspension was stirred at room temperature for 20 h. All solvents were evaporated, the remaining solids were adsorbed on silica gel and purified by column chromatography over silica gel with hexanes/CH_2Cl_2 1/2. The product fraction was collected and all solvents were evaporated. The yellow solid was dissolved in CH_2Cl_2 (10 mL) and methanol (15 mL) was added. The CH_2Cl_2 was removed under reduced pressure and a fine yellow powder precipitated. The yellow solid was filtered off through a glass frit (P4), washed with an excess of methanol and dried under vacuum. The product was obtained as bright yellow powder with a yield of 39 % (21.0 mg, 23.3 µmol).

^{1}H NMR ($CDCl_3$, 400 MHz, rt.): δ [ppm] = 9.16 (s, 2H, 1/2/3/4/5/6), 9.04 (s, 2H, 1/2/3/4/5/6), 9.02 (s, 2H, 1/2/3/4/5/6), 8.96 (s, 2H, 1/2/3/4/5/6), 8.94 (s, 2H, 1/2/3/4/5/6), 8.90 (s, 2H, 1/2/3/4/5/6), 7.42 (bs, 1H, 10), 3.90 (q, 2H, ^3J = 6.6 Hz, 11), 2.03 – 1.94 (m, 2H, 12), 1.86 (s, 9H, 9), 1.83 (s, 18H, 10/11), 1.79 (s, 18H, 10/11), 1.76 – 1.67 (m, 2H, 13) 1.19 (t, 3H, ^3J = 7.4 Hz, 14).

^{13}C NMR ($CDCl_3$, 100 MHz, rt.): δ [ppm] = 169.5, 148.4, 148.2, 132.2, 130.19, 130.17, 129.9, 129.85, 129.77, 129.4, 126.8, 123.20, 123.15, 120.6, 120.2, 119.82, 119.79, 119.0, 118.9, 118.8, 118.51, 118.48, 118.3, 40.5, 35.7, 35.63, 35.62, 32.13, 32.11, 32.0, 20.6, 14.0.

MS (MALDI-ToF, dctb): m/z = 902 $[M]^+$

HRMS (MALDI-ToF, dctb): m/z (calculated for $C_{67}H_{67}NO$): 901.5217 $[M]^+$
m/z (measured): 901.5212 $[M]^+$

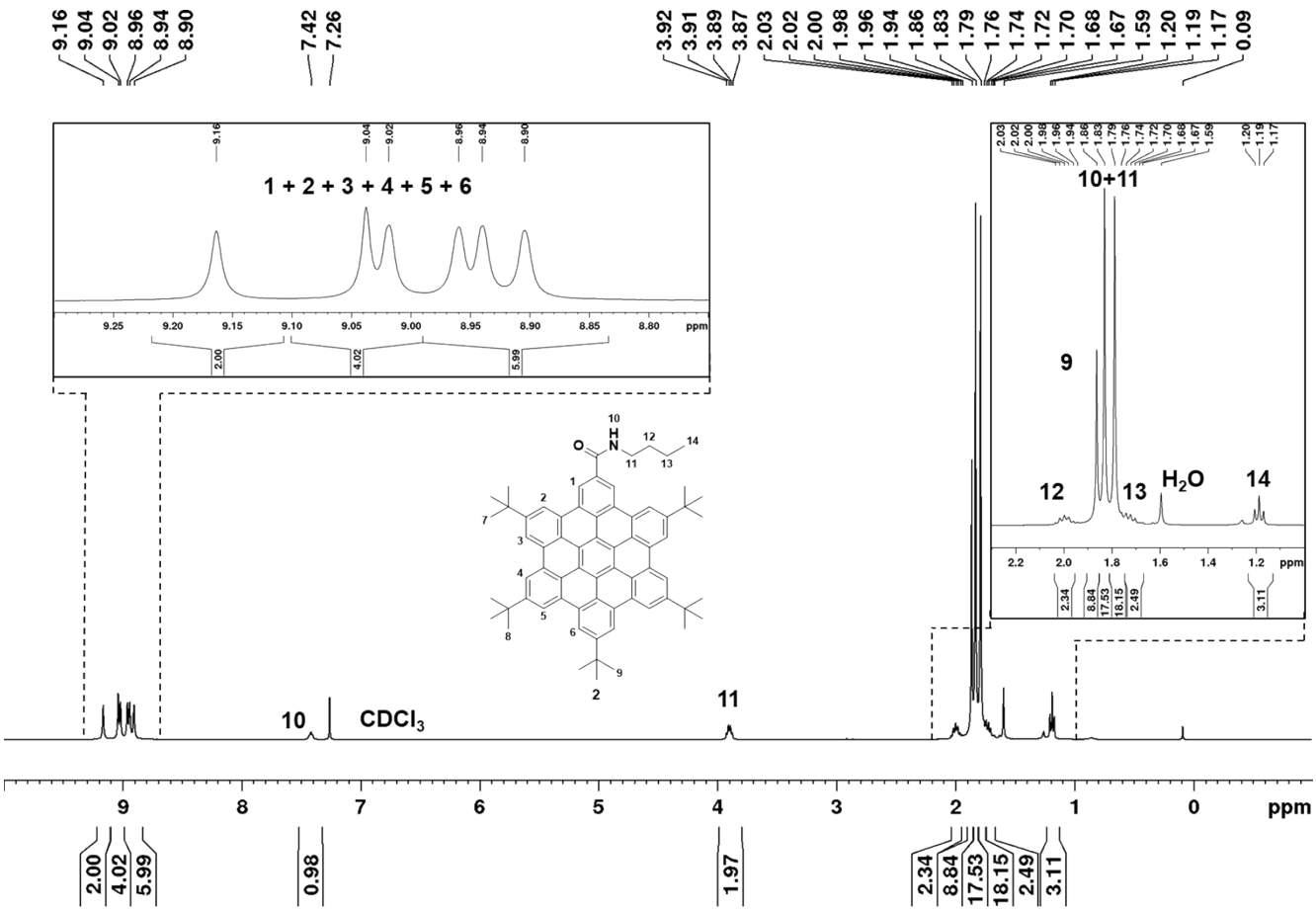

Figure S12. ^{1}H NMR spectrum of **2** in $CDCl_3$ (400 MHz, rt.).

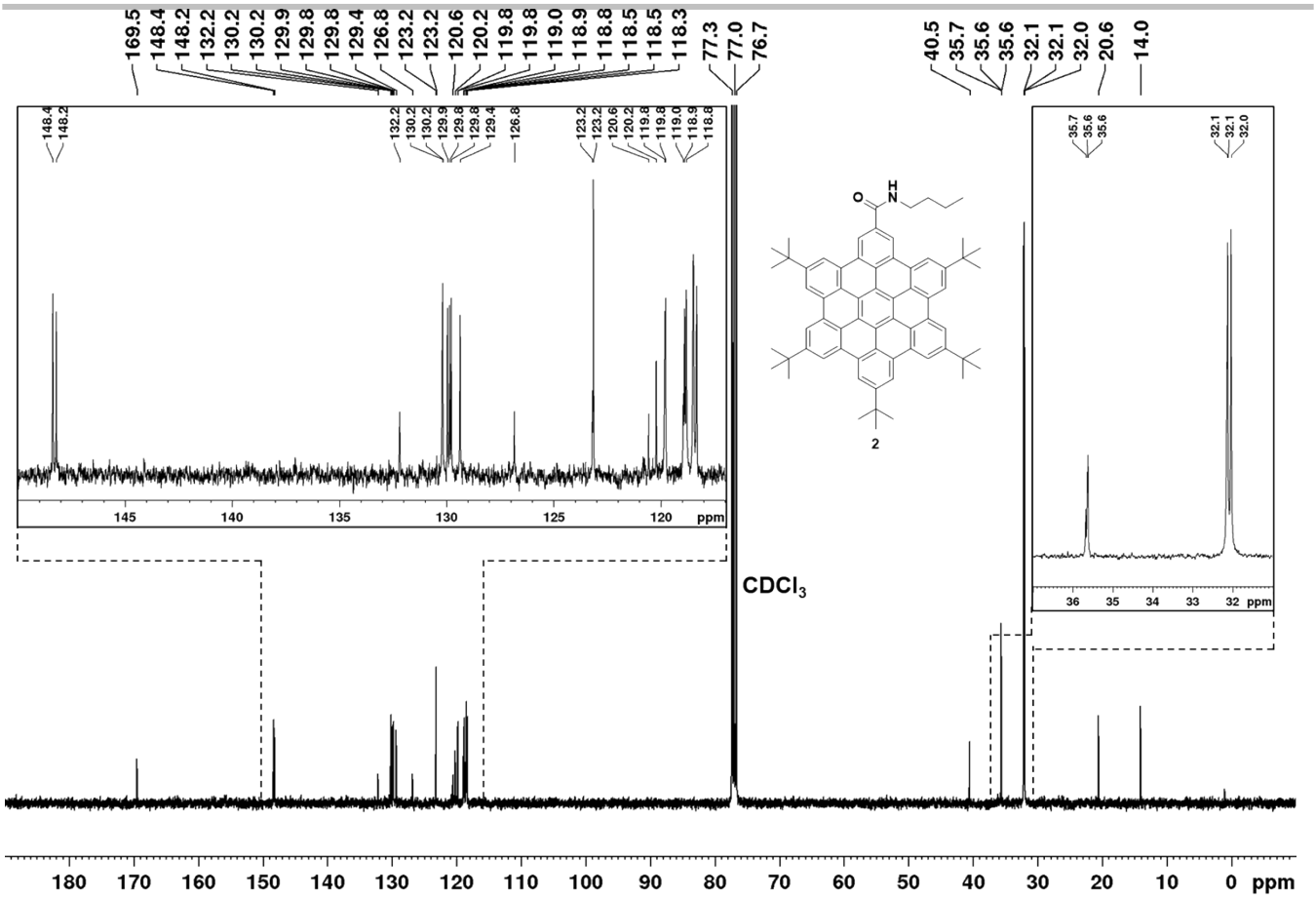

Figure S13. ^{13}C NMR spectrum of **2** in $CDCl_3$ (100 MHz, rt.).

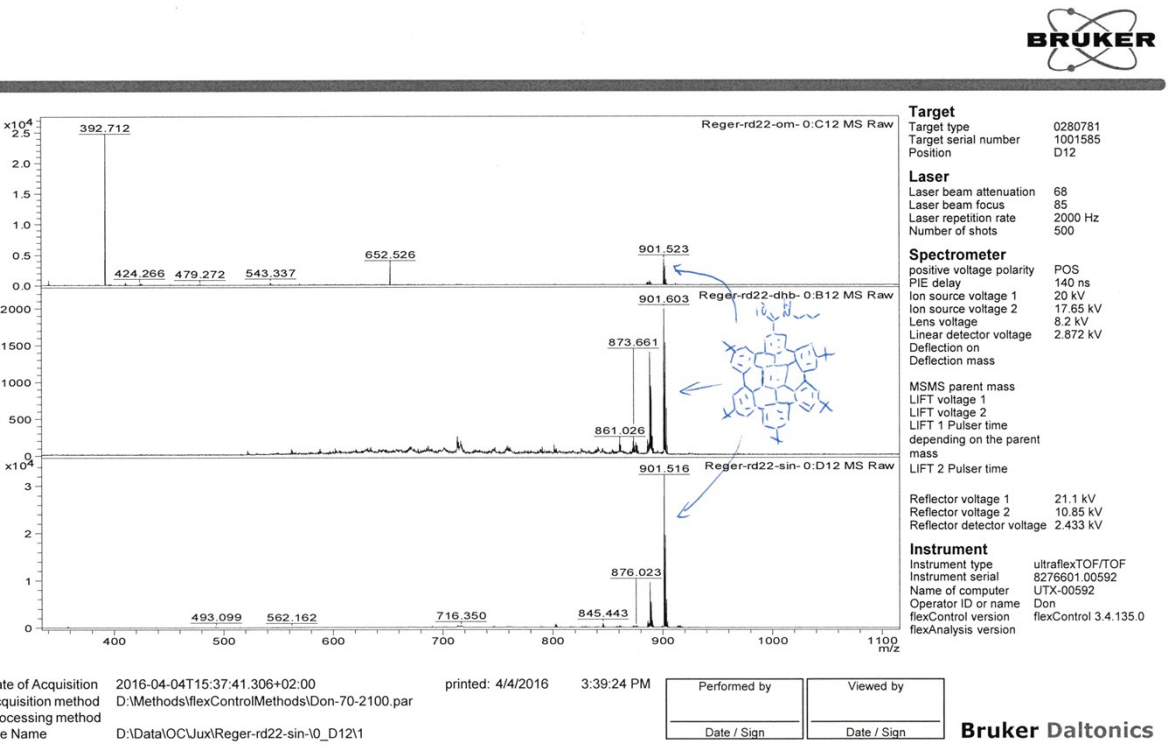

Figure S14. MALDI-ToF spectra of **2** (overview) (top: without matrix; mid: dhb; bottom: sin).

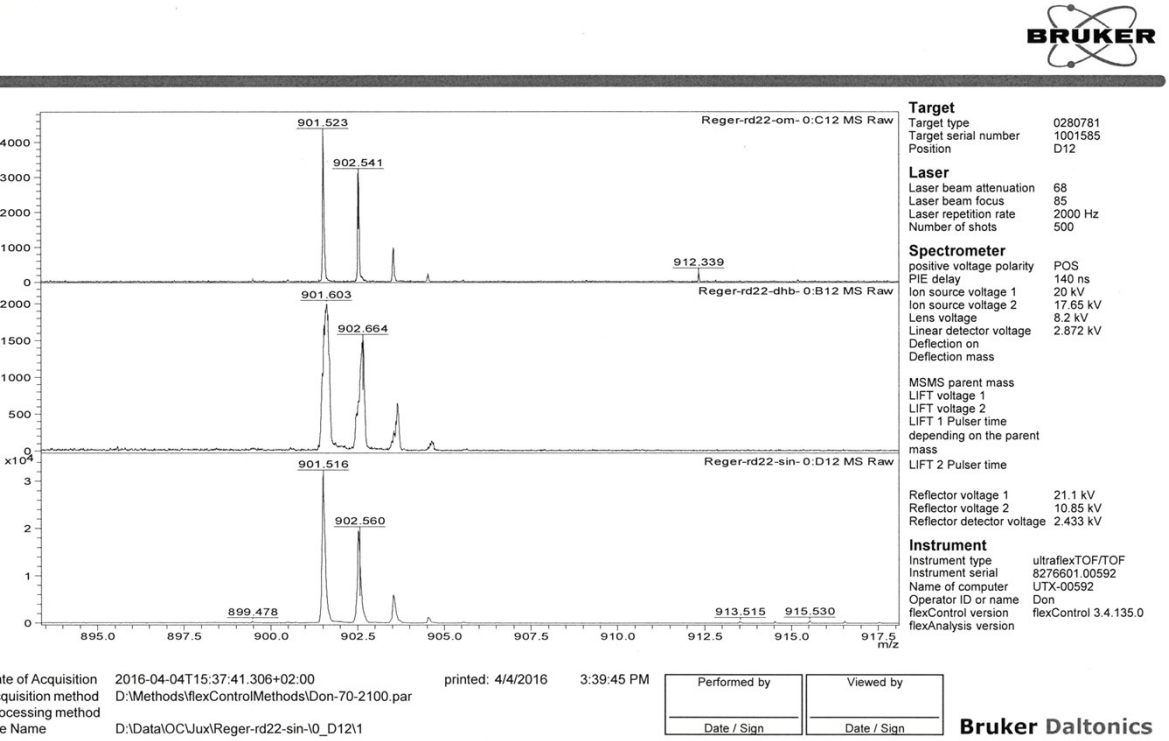

Figure S15. MALDI-ToF spectra of **2** (zoom on product peak) (top: without matrix; mid: dhb; bottom: sin).

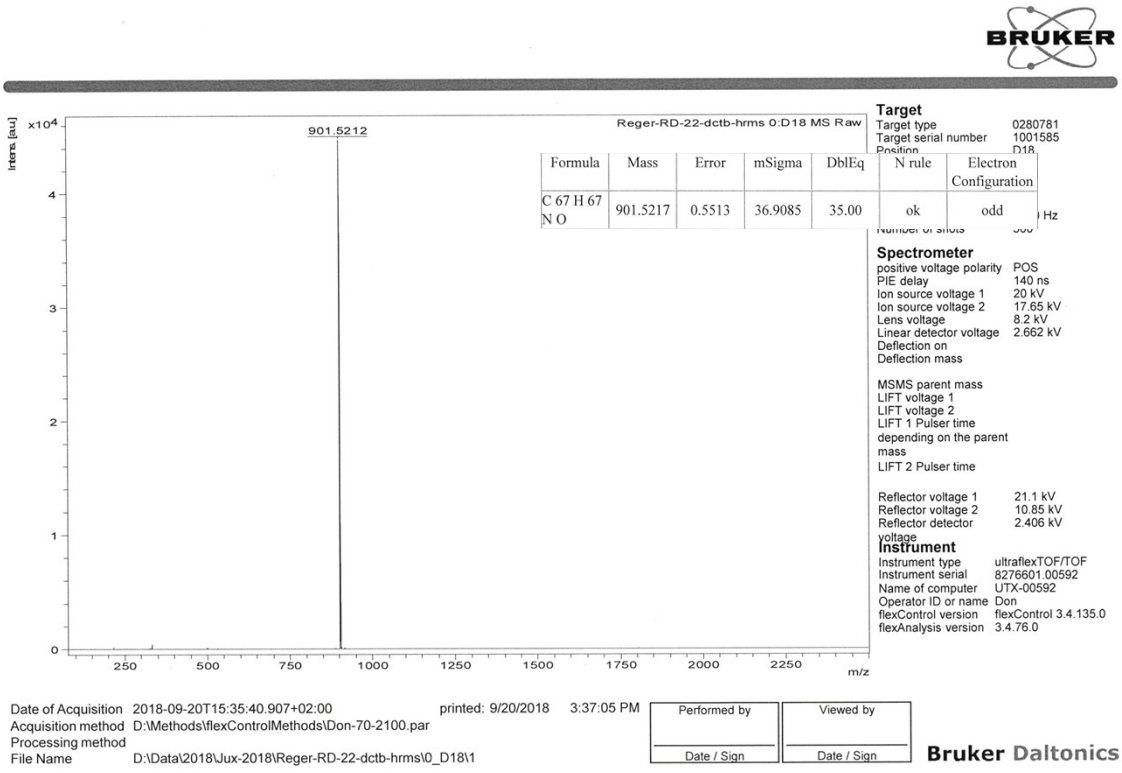

Figure S16. HRMS MALDI-ToF of **2** (overview) (dctb). Inset: Calculated mass.

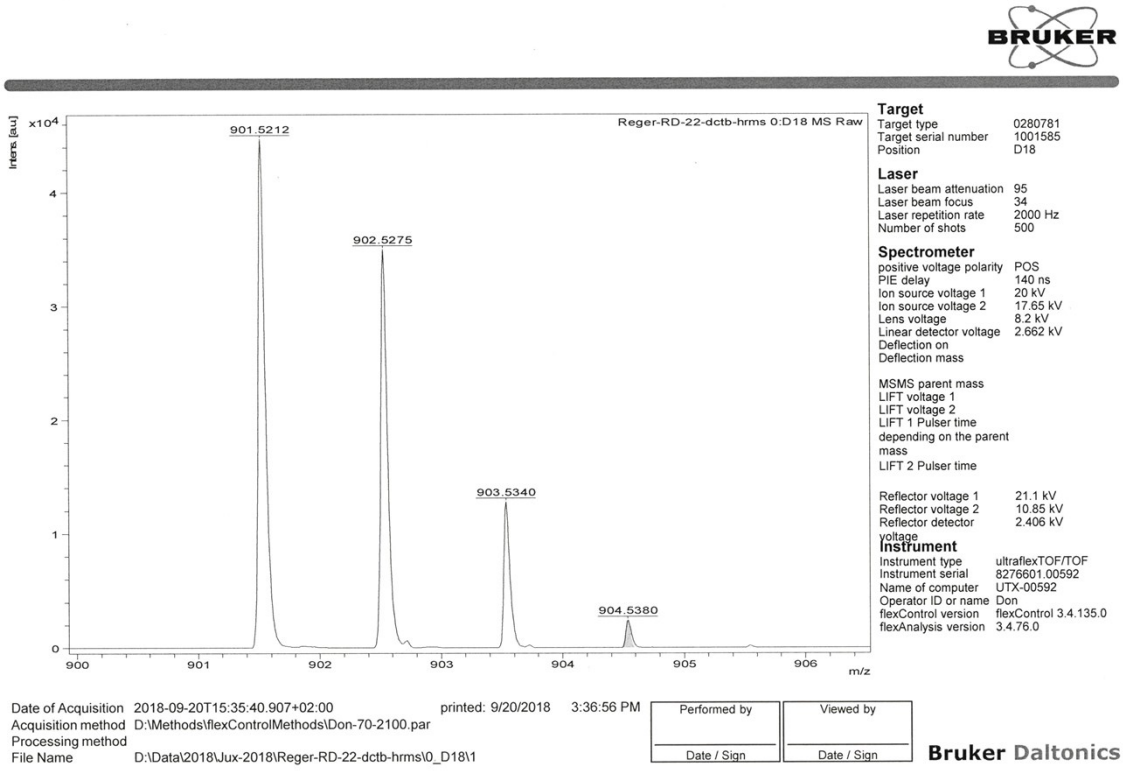

Figure S 17. HRMS MALDI-ToF of **2** (zoom on product peak) (dctb). Simulated MS as grey background.

Pentakis-tert-butyl-mono-nitro HBC (5)

A round-bottom Schlenk flask (100 mL) equipped with a magnetic stirring bar and a septum was charged **HAB-NO_2** (0.30 g, 0.35 mmol), DDQ (0.56 g, 2.45 mmol), and CH_2Cl_2 (75 mL). The mixture was degassed by N_2 bubbling for 20 min. Meanwhile the mixture was cooled to 0 °C in an ice-bath. Triflic acid (0.74 g, 0.43 mL, 4.90 mmol) was added at 0 °C. The ice bath was removed and the reaction mixture was stirred for 40 h at room temperature. It was quenched with methanol (60 mL) and a dark yellow solid precipitated. The solid was filtered off through a glass frit (P4) and washed with an excess of methanol. The solid was taken up in THF and filtered over a pad of silica gel. The product was finally purified by column chromatography over silica gel with hexanes/CH_2Cl_2 3/2. To obtain a fine powder the orange solid was dissolved in a minimal amount of CH_2Cl_2 and precipitated by addition of an excess of methanol. After filtration over a glass frit (P4) and drying under vacuum the product was obtained as an orange solid in a yield of 60% (0.18 g, 0.21 mmol)

^{1}H NMR ($CDCl_3$, 400 MHz, rt.): δ [ppm] = 9.15 (s, 2H, 1), 9.04 (s, 2H, 2/3/4/5/6), 8.96 (s, 2H, 2/3/4/5/6), 8.94 (s, 2H, 2/3/4/5/6), 8.76 (s, 2H, 2/3/4/5/6), 8.50 (s, 2H, 2/3/4/5/6), 1.97 (s, 9H, 9), 1.91 (s, 18H, 10/11), 1.75 (s, 18H, 10/11).

^{13}C NMR ($CDCl_3$, 100 MHz, rt.): δ [ppm] = 149.2, 148.6, 148.4, 144.9, 130.3, 129.7, 129.6, 129.4, 128.4, 128.0, 122.9, 122.8, 122.7, 121.0, 120.1, 119.5, 119.1, 118.9, 118.72, 118.65, 118.5, 117.6, 114.6, 35.9, 35.7, 35.5, 32.1, 32.0.

MS (MALDI-ToF, dhb): m/z = 847 $[M]^+$

HRMS (APPI): m/z (calculated for $C_{62}H_{57}NO_2$): 847.438381 $[M]^+$
m/z (measured): 847.439506 $[M]^+$

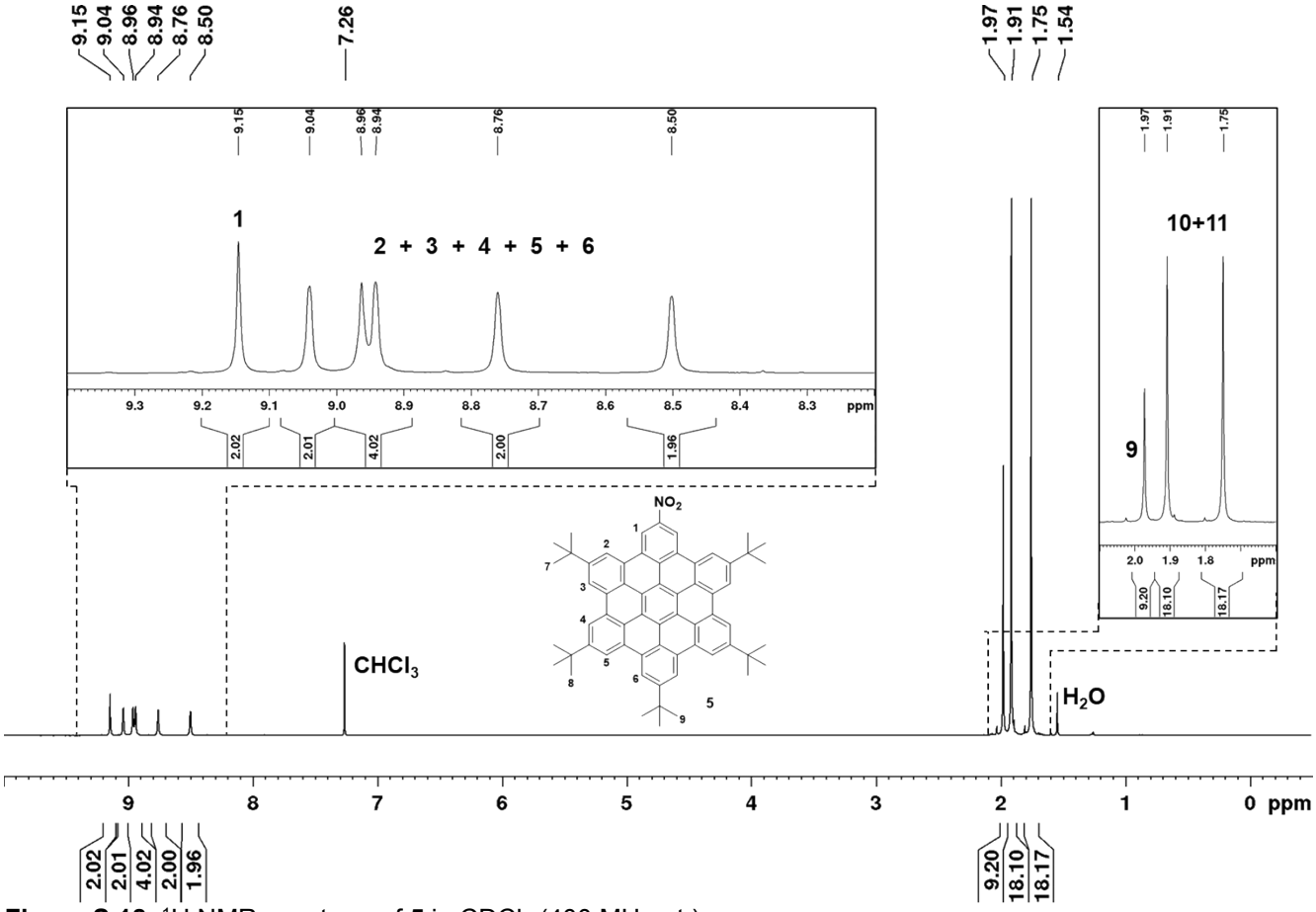

Figure S 18. ^{1}H NMR spectrum of **5** in $CDCl_3$ (400 MHz, rt.).

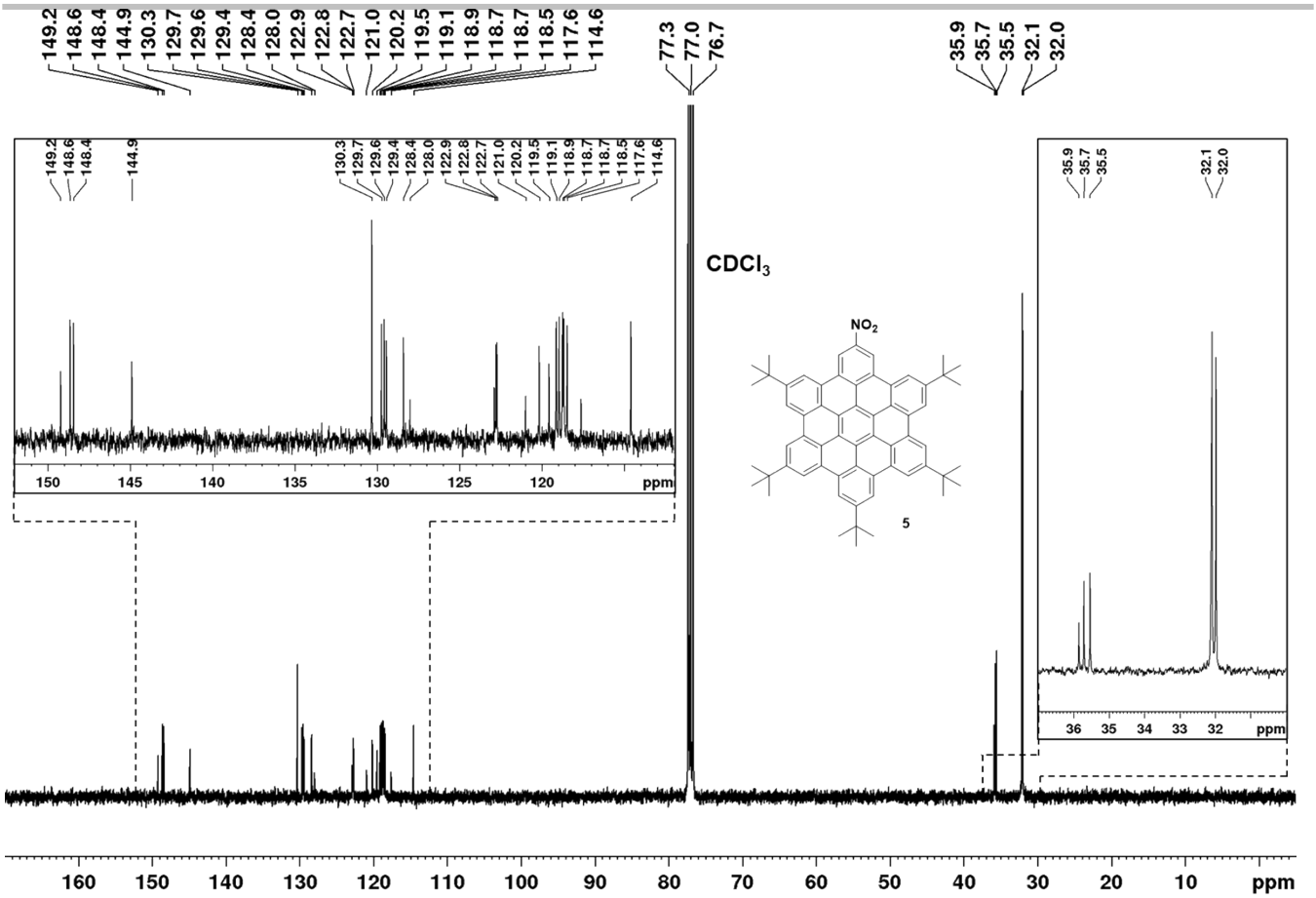

Figure S19. ^{13}C NMR spectrum of **5** in $CDCl_3$ (100 MHz, rt.).

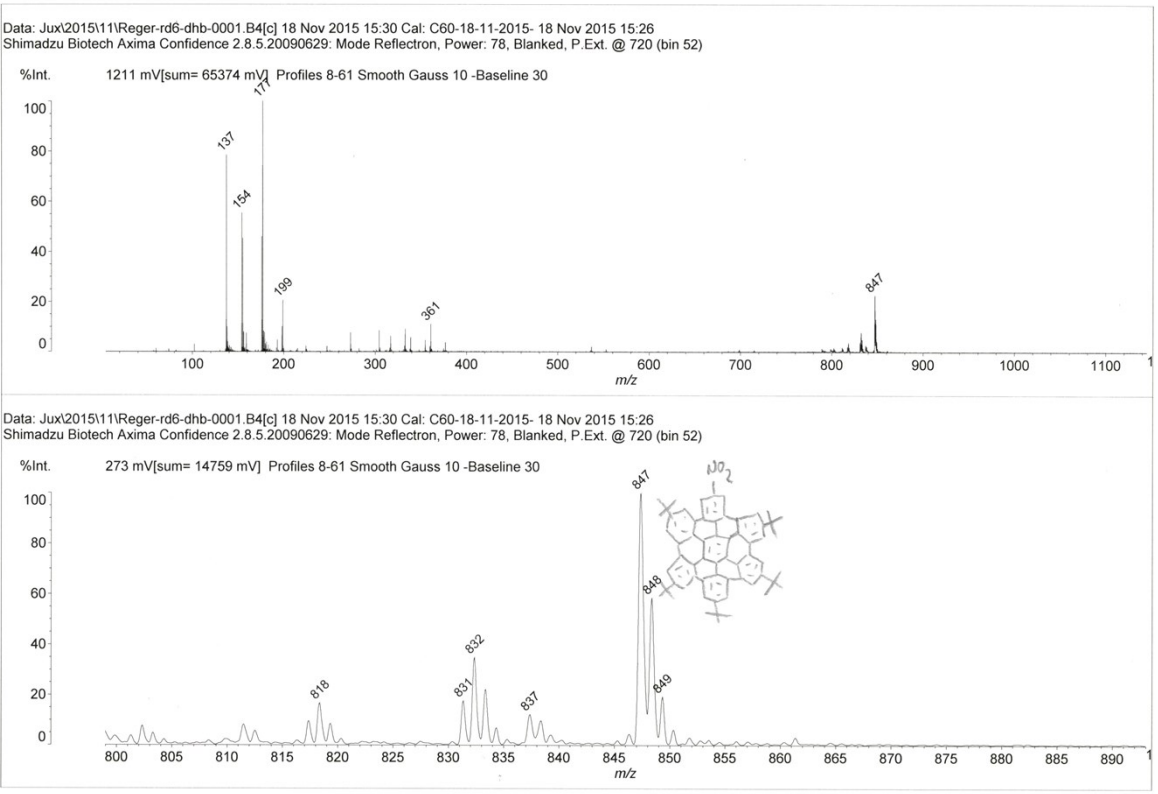

Figure S 20. MALDI-ToF spectrum of **5** (dhb) (top: overview; bottom: zoom on product peak).

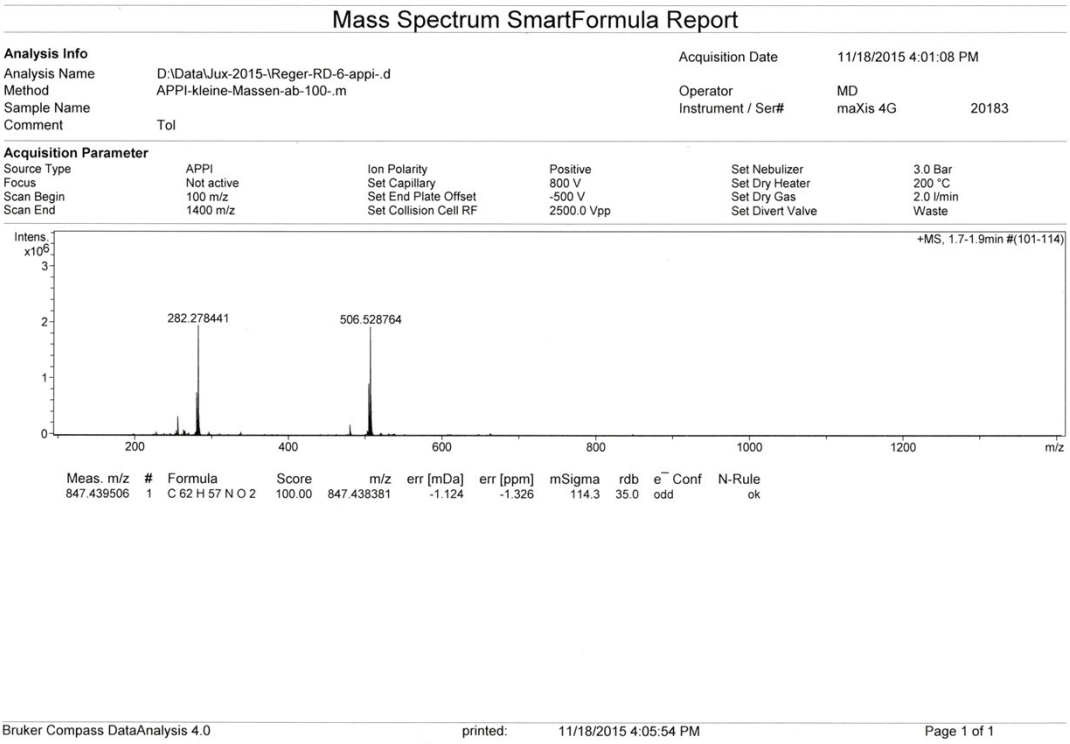

Figure S 21. HRMS (APPI, toluene) of **5** (overview).

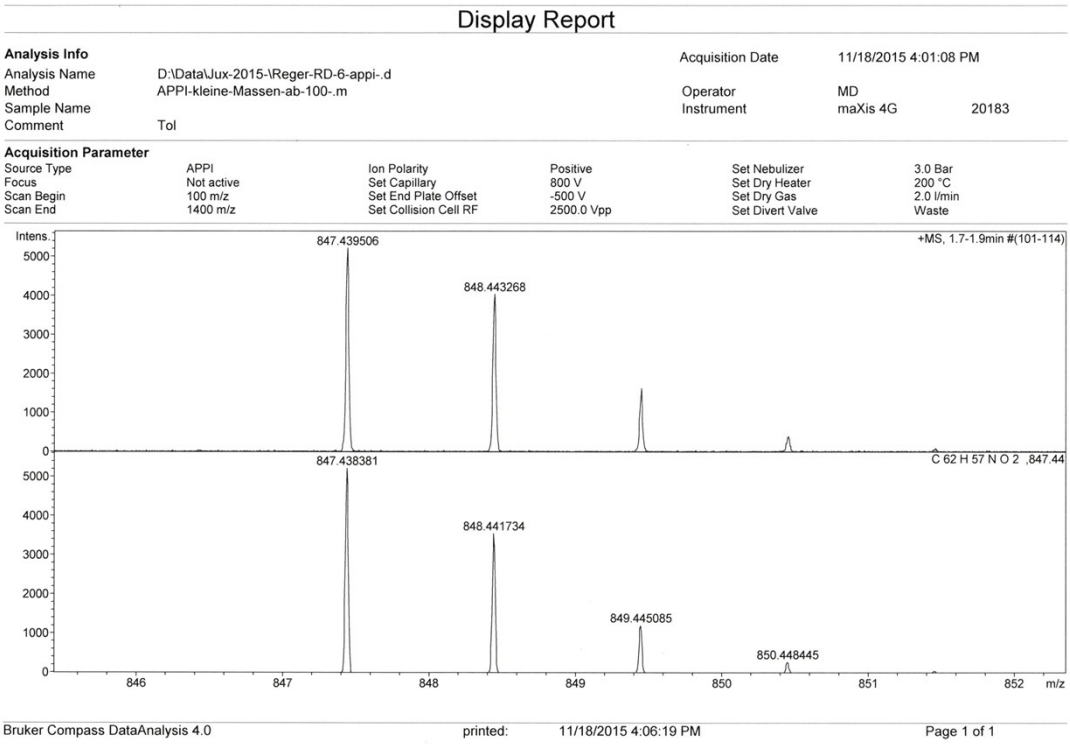

Figure S 22. HRMS (APPI, toluene) of **5** (top: measured; bottom: calculated).

Calculations

For further support of the experimental data and to describe the excited state characteristics of the **HBC**s, we performed time-dependent DFT (TD-DFT) calculations. All calculations were carried out with the Gaussian09 Revision D.01 code.[1] To account properly for possible CT states, we employed the range-separated hybrid functional CAM-B3LYP, since it performs much better in describing long-range electron-hole interactions than normal hybrid functionals such as B3LYP.[2] For geometry optimizations and single point calculations (energies, spectra) we used the Pople double-zeta basis sets 6-31G* and 6-31+G* including diffuse functions, respectively.
Since the steady-state and time-resolved experiments point to a CT state as the first excited singlet state in case of **5**, but not in case of **1** – **4**, we calculated the transition energies upon vertical excitation and the ground and excited state electron densities in different environments of varying polarity. Calculations were performed in vacuum and solution (THF, benzonitrile) with the polarized continuum model (PCM). Note that a solvent can react in two ways on re-distributions of the electron density of a solute: Firstly, by a polarization of its electron density, which is a very fast process. Secondly, by a reorientation of solvent molecules, which is a comparably slow process. Hence, we exclude the latter contribution from the transition energy of vertical excitation (analogous to the relaxation of the excited state geometry). To put it plainly, we used the static dielectric constants for ground state geometry optimizations and energy calculations (ε_{stat}(THF) = 7.4257, ε_{stat}(benzonitrile) = 25.5920) and the dynamic dielectric constants for energy calculations of the first excited state (ε_{dyn}(THF) = 1.9740, ε_{dyn}(benzonitrile) = 2.3375). Instead of the faster but less accurate linear-response method for transition energies, we applied the state-specific approach, in which the mutual changes of solute electron density re-distribution and solvent polarization are treated iteratively until self-consistency is reached. The transition energies are then obtained from the difference of the excited and ground state energy.
The results of our calculations are summarized in table S1. The transition energies to the first excited singlet state of **1** – **3** are independent from polarity of the environment. In contrast, we observe a slight red-shift for **4** and a strong red-shift for **5** when going from the totally nonpolar vacuum to THF or benzonitrile solvation. Furthermore, we found that the oscillator strength of the $S_0 \rightarrow S_1$ transition is zero in case of **1**, which is due to its symmetric substituents as discussed in the experimental section. To quantify the extent of the first excited state CT character, we analyzed the electron density re-distribution (difference between excited and ground state electron density) upon excitation with the method of Le Bahers et al.[3] Briefly explained, their method ascribes barycenters to the regions of electron density depletion/increase and quantifies the CT character with the excitation length D(CT), amount of transferred charge q(CT), and the change between excited and ground state dipole moment $\Delta\mu(CT) = q(CT) \times D(CT)$ (the latter value corresponds to the difference of the excited and ground state dipole moments, which were also obtained directly from the calculations and are also listed in table S1). As expected, all of these values increase with increasing strength of the –M-effect and the environment polarity. However, the values obtained for **5** are significantly increased as compared to the other **HBC** derivatives. The most demonstrative value is certainly q(CT), which amounts to 0.819 e for **5** in benzonitrile, meaning that almost the full charge of an electron is transferred from the **HBC** π-system to the nitro-group upon excitation. Hence, our calculations indicate a strong CT character of the first excited state of **5** and are in excellent agreement with our experimental results.

Table S 1. Excitation energy E(S_0 → S_1), oscillator strength f, CT excitation length D(CT), transferred charge q(CT), change between excited and ground state dipole moment Δμ(CT), excited state dipole moment μ(ES), ground state dipole moment μ(GS), and difference between excited and ground state dipole moment Δμ(ES – GS) (see text for definitions and values). The three values in each cell were obtained from calculations in vacuum, THF, and benzonitrile.

HBC	1	2	3	4	5
E(S_0 → S_1) [eV]	3.305 3.311 3.312	3.284 3.287 3.280	3.257 3.240 3.238	3.228 3.178 3.171	3.161 2.641 2.482
E(S_0 → S_1) [nm]	375 374 374	377 377 378	380 382 382	384 390 391	392 469 499
f	0.000 0.000 0.000	0.003 0.003 0.003	0.013 0.014 0.014	0.017 0.024 0.026	0.027 0.044 0.044
D(CT) [Å]	0.093 0.033 0.055	0.559 0.708 0.745	0.817 1.018 1.040	1.162 1.445 1.478	1.998 2.634 2.694
q(CT) [e]	0.239 0.240 0.240	0.258 0.264 0.265	0.288 0.301 0.303	0.320 0.357 0.364	0.452 0.766 0.819
Δμ(CT) [D]	0.107 0.038 0.064	0.691 0.898 0.950	1.131 1.473 1.514	1.788 2.480 2.583	4.326 9.695 10.599
μ(ES) [D]	0.109 0.205 0.235	4.150 6.103 6.572	4.315 5.931 6.242	6.641 9.022 9.439	11.581 20.154 21.829
μ(GS) [D]	0.058 0.126 0.150	3.857 5.510 5.921	3.259 4.292 4.495	5.006 6.307 6.527	7.239 8.909 9.167
Δμ(ES-GS) [D]	0.051 0.079 0.086	0.293 0.593 0.652	1.056 1.640 1.747	1.634 2.715 2.912	4.342 11.245 12.662

Steady state absorption & fluorescence spectroscopy

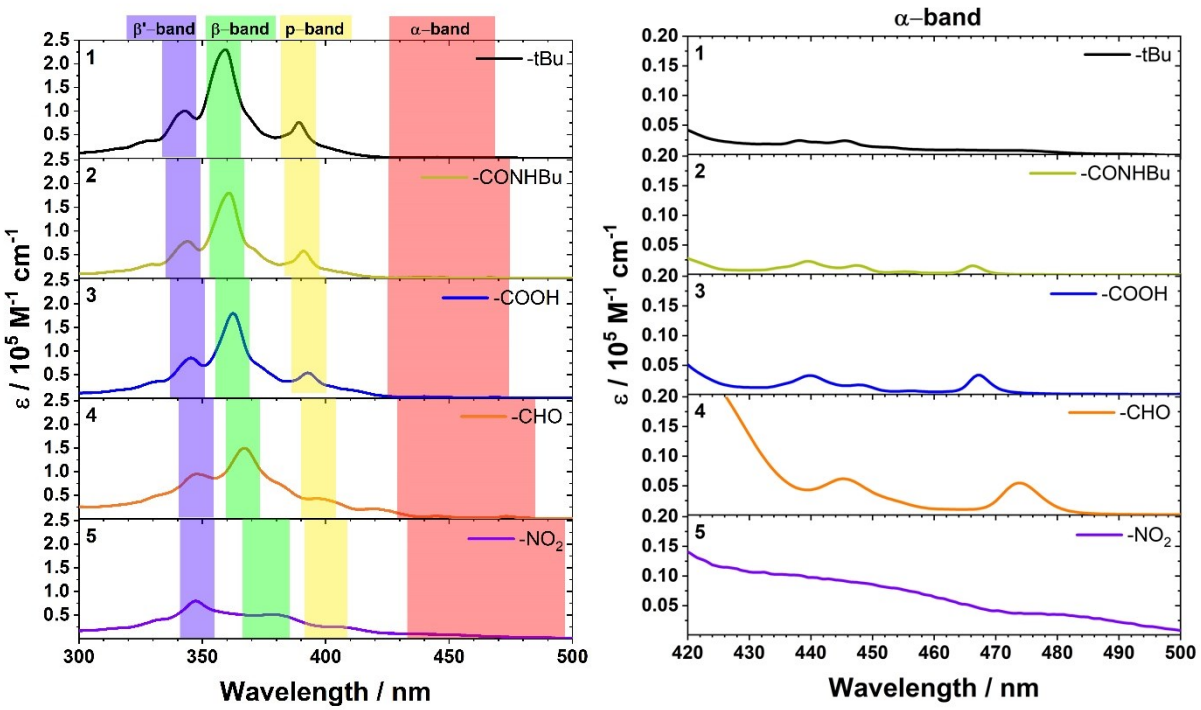

Figure S23. Left: Assignment of the observed absorption bands to the nomenclature according to Clar's rule.[4–6] Right: Enlarged presentation of the α-absorption bands to show their enhancement with the stronger -M-effect.

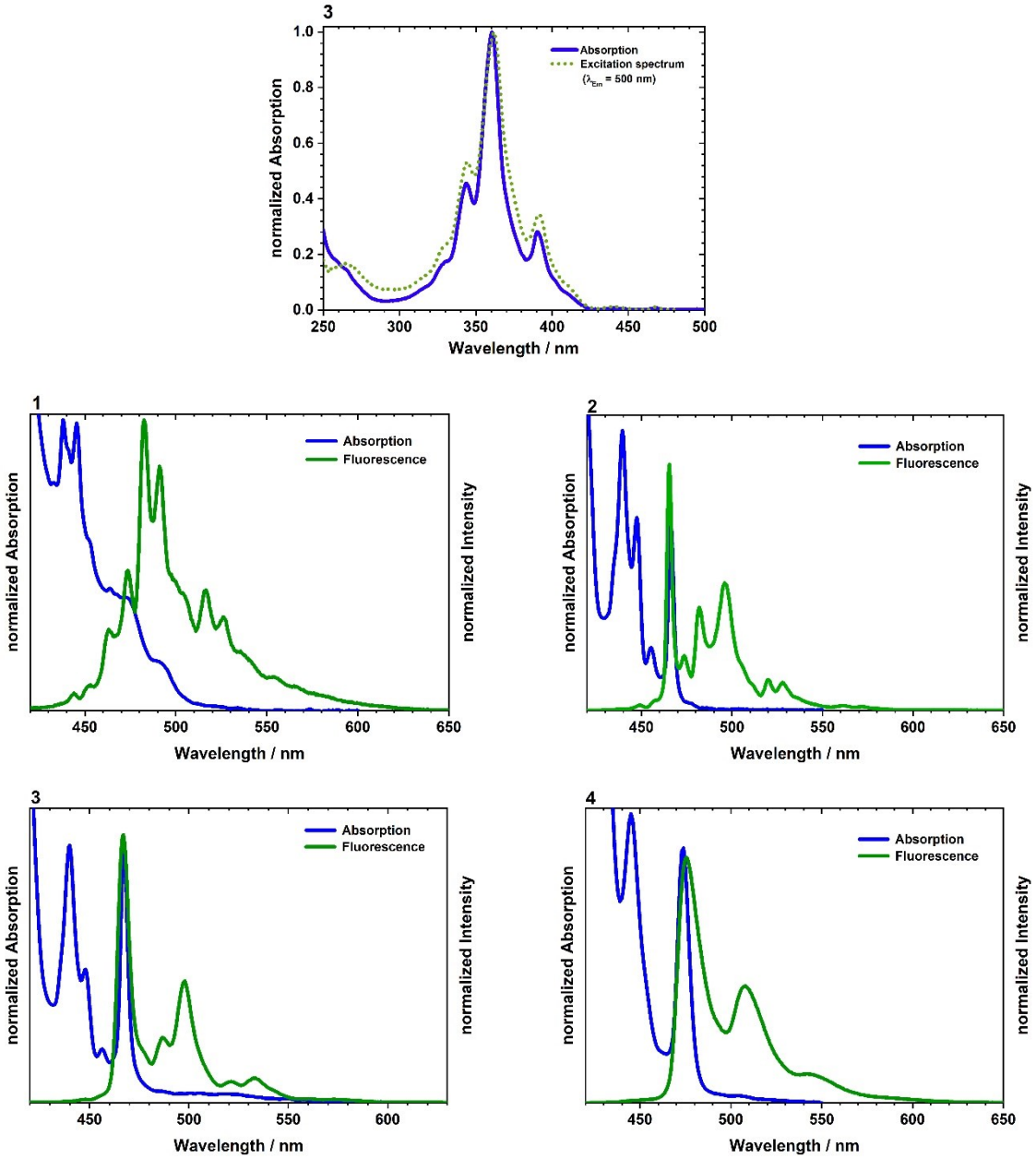

Figure S24. Top: Absorption Correlated fluorescence–excitation spectrum (green dotted spectra) representatively shown for 3. The steady-state absorption spectra is shown in blue. The excitation spectrum was recorded for the fluorescence 500 nm. Middle Left: Comparison of the α-absorption bands and the mirror-imaged fluorescence shown for 1. Fluorescence was obtained upon excitation at 350 nm. Middle Right: Comparison of the α-absorption bands and the mirror-imaged fluorescence shown for 2. Fluorescence was obtained upon excitation at 350 nm. Bottom Left: Comparison of the α-absorption bands and the mirror-imaged fluorescence shown for 3. Fluorescence was obtained upon excitation at 350 nm. Bottom Right: Comparison of the α-absorption bands and the mirror-imaged fluorescence shown for 4. Fluorescence was obtained upon excitation at 350 nm.

Table S 2. Summary of absorption bands of **1–5** in THF.

HBC	Absorption / nm			
	β'-band	**β-band**	**p-band**	**α-bands**
1	343.0	359.0	389.0	438.0 445.5 468.0 489.5
2	344.5	361.0	391.0	439.5 447.5 464.5
3	345.5	362.5	393.0	440.0 448.0 456.5 467.0
4	347.5	367.0	396.5	445.0 474.0
5	347.5	378.5	401.5	439.0 476.5

Quantum yields are determined by the according to the instructions of 'A Guide to Recording Fluorescence Quantum Yields' from Horiba. Hereby, steady-state absorption and emission (with fixed excitation wavelength) of differently concentrated samples of the compound and the reference are measured. The emission spectra of the different concentrations are integrated and plotted against the absorbance at the excitation wavelength. The obtained datapoints should have a linear order. With the resulting gradient and the refractive indices of the used solvents, the fluorescence quantum yield can be determined with the following equation: $\Phi_{Sample} = \Phi_{Reference} \times \left(\frac{Gradient_{Sample}}{Gradient_{Reference}}\right) \times \left(\frac{\eta^2_{Sample}}{\eta^2_{Reference}}\right)$ The error typically ranges by ±10% based on the errors occurring by the determination of the gradients.

Table S3. Quantum yields of **1** – **5** in THF at ambient conditions. The excitation wavelength λ_{Exc} is 350 nm and diphenylanthracene in ethanol (Φ_{Fl} = 0.95) was used as reference.

Compound	Φ_{Fl} / %
1	4.1 (±0.5)
2	4.2 (±0.2)
3	7.7 (±0.4)
4	9.7 (±0.6)
5	8.7 (±0.2)

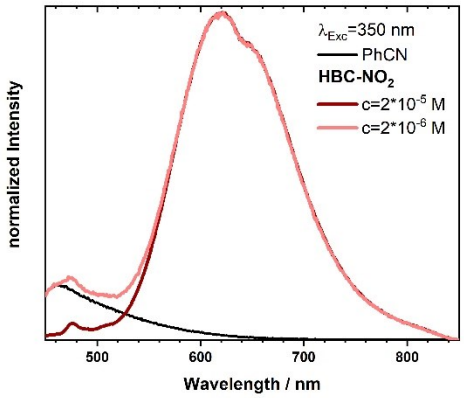

Figure S25. Normalized steady-state fluorescence spectra of 5 in benzonitrile (λ_{Exc} = 350 nm) at high (c = 2×10^{-5} M; dark red) and low concentrations (2×10^{-6} M ; light red). The corresponding spectrum of pure benzonitrile (black) is illustrated to show that the spectral changes in the low wavelength area are purely solvent-related.

Solvent-dependent emission

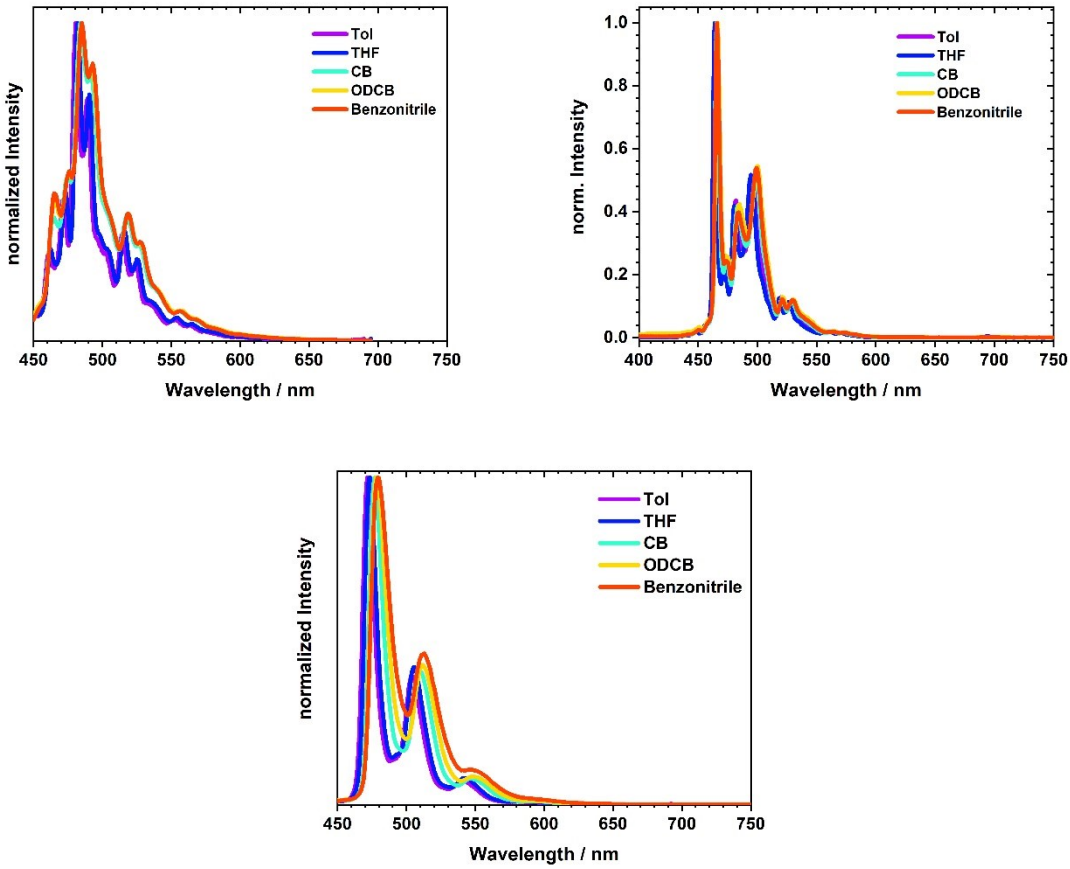

Figure S26. Normalized fluorescence spectra of 1 (top left), 2 (top right) and 4 (bottom) in toluene (Tol), tetrahydrofuran (THF), chlorobenzene (CB), 1,2-dichlorobenzene (ODCB), and benzonitrile upon excitation at 350 nm at room temperature.

Table S4. Quantum yields of 5 in different solvents with corresponding E_T^N values.[7] E_T^N values are defined as dimensionless quantity relative to water and tetramethylsilane as polar and nonpolar reference. The excitation wavelength λ_{Exc} is 350 nm.

Solvent	E_T^N	Φ_{Fl} / %
Tol	0.099	7.3 (±0.3)
CB	0.188	9.6 (±0.4)
THF	0.207	8.7 (±0.5)
ODCB	0.225	4.8 (±0.4)
PhCN	0.333	1.0 (±0.4)

Temperature-dependent emission

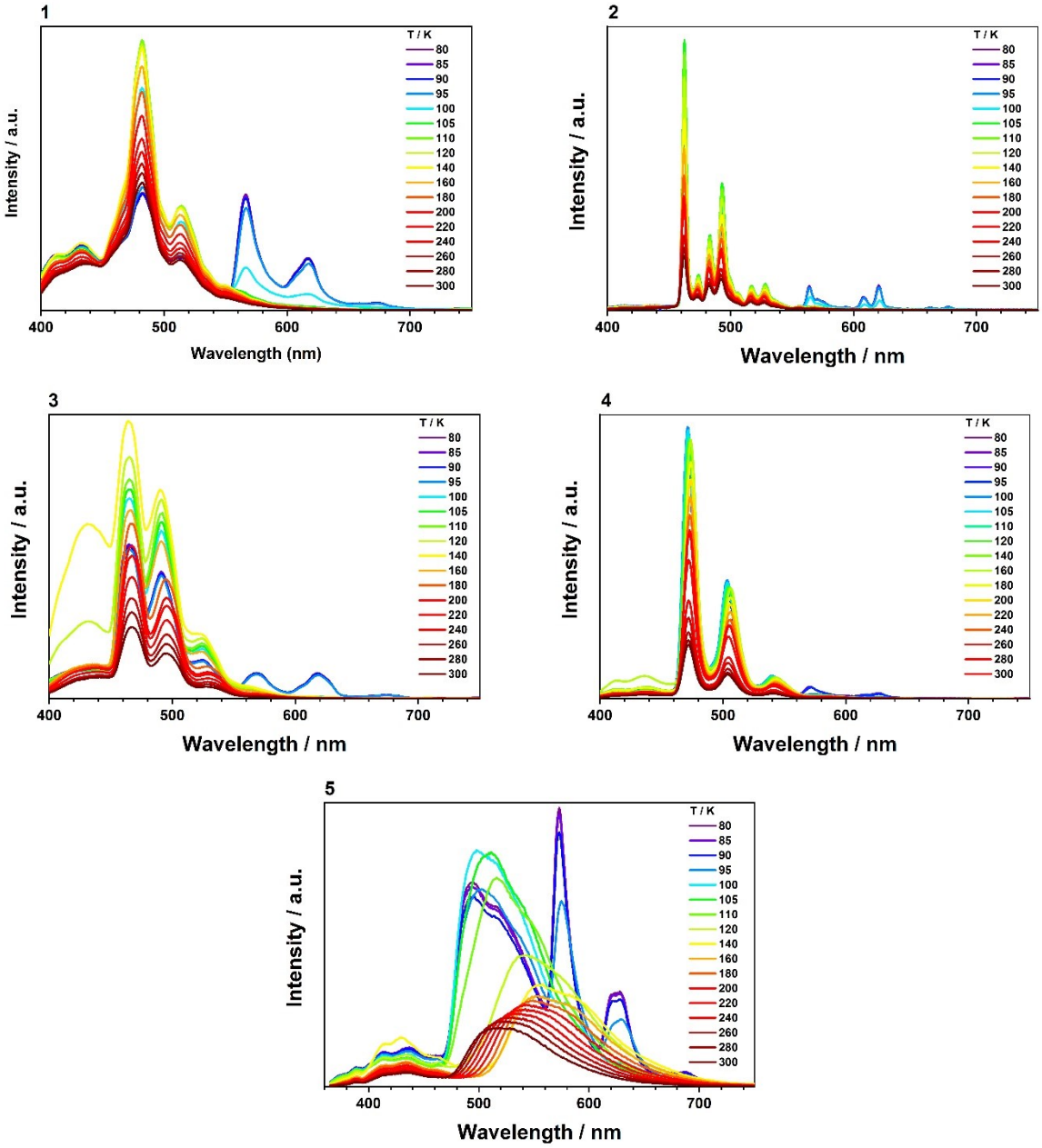

Figure S27. Temperature-dependent emission spectra of 1 (upper left), 2 (upper right), 3 (middle left), and 4 (middle right) and 5 (bottom) in 2-MeTHF upon excitation at 350 nm at different temperatures between 80 and 297 K (from purple to red). The emission bands in the range below 460 nm belong to 2-MeTHF.

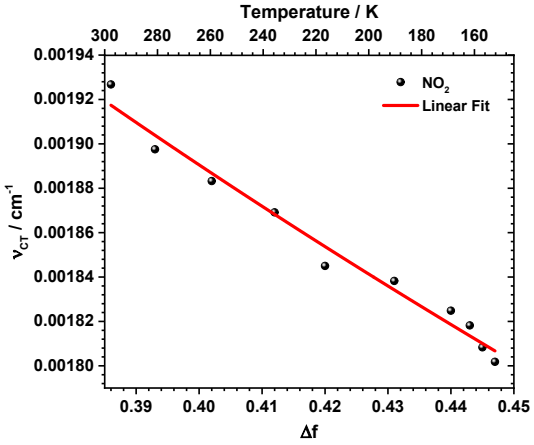

Figure S28 Lippert-Mataga plot of the thermochromic shifts in the emission of 5 in 2-MeTHF at temperatures between 150 and 300 K. The Δf values are from literature.[8]

Time-dependent emission spectroscopy

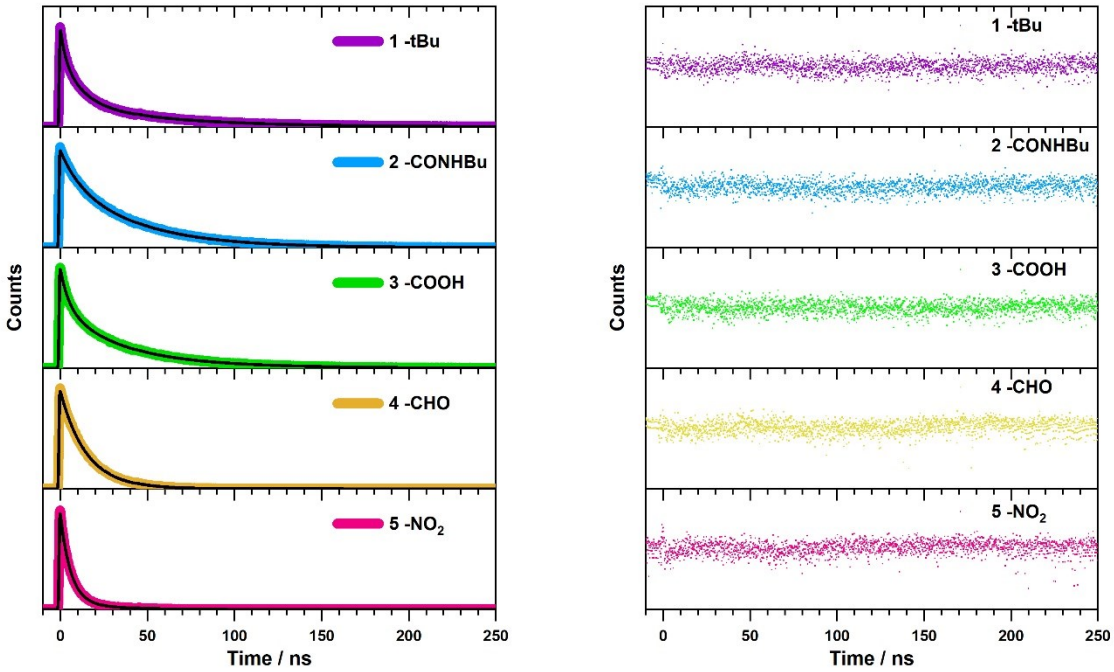

Figure S29. Left: TCSPC decay and fit (in black) of 1 (-tBu, purple, λ_{Em} = 485 nm), 2 (-CONHBu, blue, λ_{Em} = 465 nm), 3 (-COOH, green, λ_{Em} = 480 nm), 4 (-CHO, yellow, λ_{Em} = 480 nm) and 5 (-NO_2, pink, λ_{Em} = 530 nm) in THF obtained by time-correlated single photon counting upon excitation at 405 nm. Right: The corresponding residuals to the TCSPC fits.

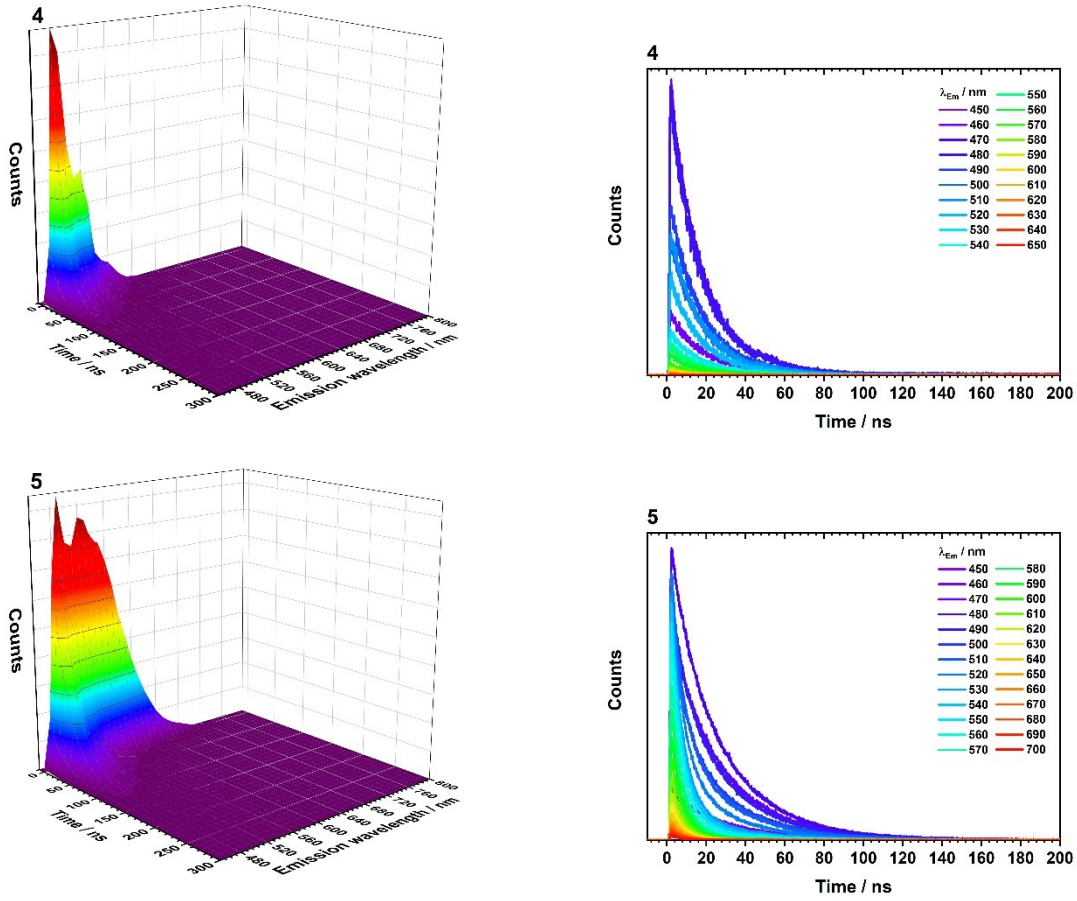

Figure S30. Time-resolved emission spectroscopy (TRES) of 4 (up) and 5 (down) (5×10^{-5} M) in THF obtained upon excitation with 405 nm laser pulses in two different presentations at room temperature. On the left, the 3D maps of the TRES measurements are shown, on the right, the corresponding 2D lifetime profiles of each emission wavelength are plotted. 4 and 5 deactivate faster at longer emission wavelengths, which are in the range of the CT emission. However, in 4, the intensity of the short-lived component is very low compared to the long-lived component.

Table S5. Excited state lifetimes of 1 – 5 in THF obtained by TCSPC upon excitation at 405 nm or transient absorption spectroscopy upon excitation at 387 nm. The latter were received by Global Analysis. τ_S is the lifetime of the singlet transients, τ_{CT} is the lifetime of the charge transfer transients. All measurements were performed at room temperature.

HBC	TCSPC			TAS	
	τ_1 / ns	τ_2 / ns	τ_3 / ns	τ_S / ns	τ_S / ns
1	1.94	**9.53**	**47.07**	**11.69**	**54.67**
2	2.29	**8.22**	**40.62**	**8.67**	**41.06**
3	2.24	**8.62**	**37.77**	**8.06**	**39.78**
HBC	**TCSPC**			**TAS**	
	τ_{CT} / ns		τ_S / ns	τ_{CT} / ns	τ_S / ns
4	5.41		**17.90**		**18.43**
5	**5.69**		25.86	**4.26**	

Voltammetry

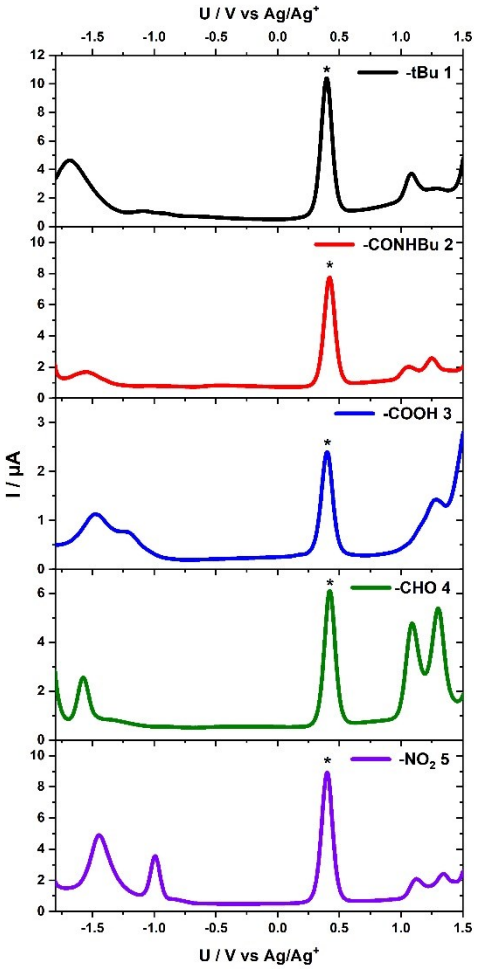

Figure S31. Differential pulse voltammograms of 1 (-tBu, black), 2 (-CONHBu, red), 3 (-COOH, blue), 4 (-CHO, green) and 5 ($-NO_2$, purple) (1 × E-3 M) in 0.2 M $TBAPF_6$ in DCM versus Fc^+/Fc at room temperature.

Table S6. Electrochemical redox potentials of 1 - 5 vs. Fc^+/Fc (0.4 V vs. SHE) obtained by differential pulse voltammetry in 0.2 M $TBAPF_6$/DCM as electrolyte. The electrochemical potentials are compared to the energy of the highest-energetic fluorescence features.

HBC	Reduction		Oxidation		Fluorescence
	E_{Red1} [V]	E_{Red1} [V]	E_{Ox1} [V]	E_{Ox2} [V]	E [eV]
1	-	-1.68	1.08	1.31	2.68 (463 nm)
2	-	-1.54	1.07	1.26	2.66 (465 nm)
3	-1.48	-1.24 (aggr.)	1.15	1.28	2.65 (467 nm)
4	-	-1.55	1.09	1.30	2.62 (473 nm)
5	-1.45	-0.99	1.12	1.34	2.01 (618 nm)

Transient absorption spectroscopy

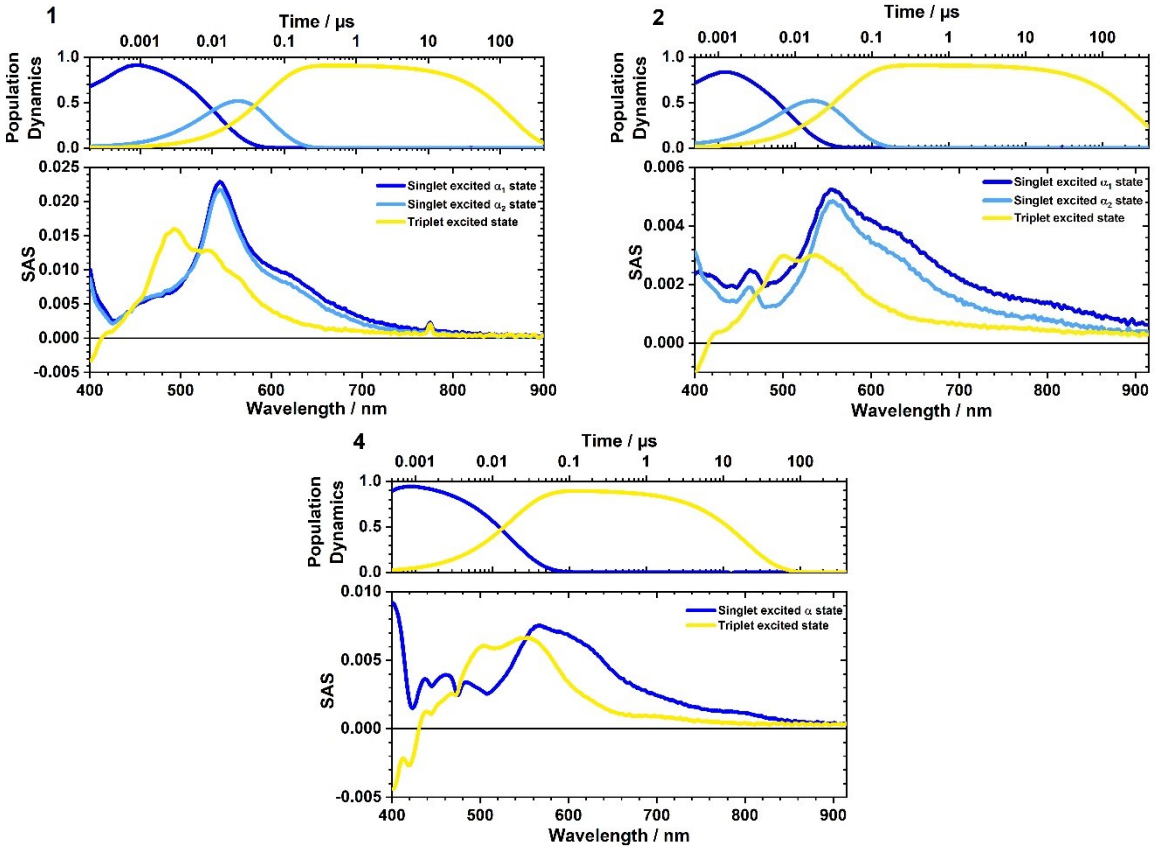

Figure S32. Top left: Species associated spectra of 1 (5×10^{-5} M) in THF with time delays of 0 and 400 µs obtained upon excitation with 387 nm laser pulses at room temperature; Top right: Species associated spectra of 2 (5×10^{-5} M) in THF with time delays of 0 and 400 µs obtained upon excitation with 387 nm laser pulses at room temperature; Bottom: Species associated spectra of 4 (5×10^{-5} M) in THF with time delays of 0 and 400 µs obtained upon excitation with 387 nm laser pulses at room temperature.

Table S7. Lifetimes obtained from the transient absorption spectroscopy measurements of 1 - 5 in THF with time delays of 0 and 400 µs upon excitation with 387 nm at room temperature determined by target analysis. τ_{CT} is the lifetime of the charge transfer state, $\tau_{S\alpha1}$ and $\tau_{S\alpha2}$ are the lifetimes of the singlet excited α state, τ_T are the lifetime of the triplet excited state transients.

HBC	τ_{CT} [ns]	$\tau_{S\alpha1}$ [ns]	$\tau_{S\alpha2}$ [ns]	τ_T [µs]
1		11.69	54.67	141.4
2		8.67	41.06	61.3
3		8.06	39.78	120.7
4			18.43	19.5
5	5.30			15.0

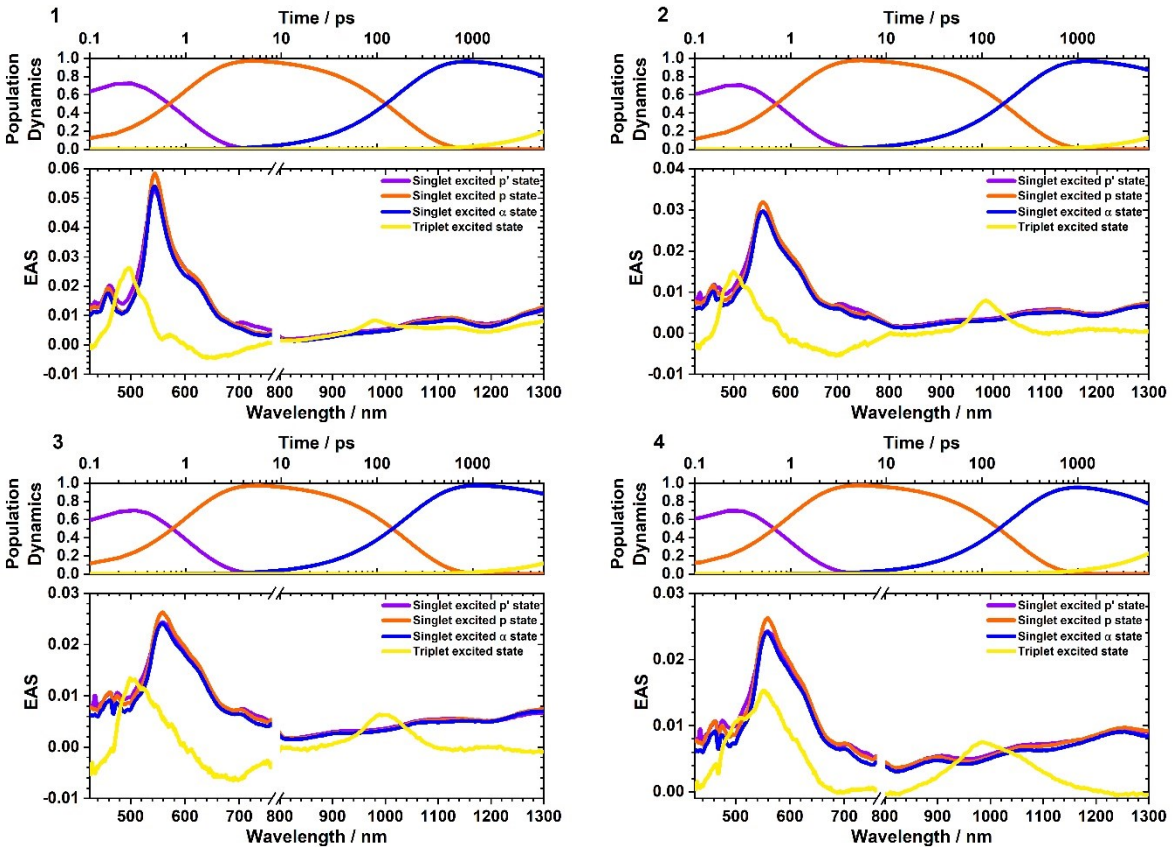

Figure S33. Top left: Evolution associated spectra of 1 (5 × 10^{-5} M) in THF with time delays of 0 and 5500 ps obtained upon excitation with 387 nm laser pulses at room temperature.; Top right: Evolution associated spectra of 2 (5 × 10^{-5} M) in THF with time delays of 0 and 5500 ps obtained upon excitation with 387 nm laser pulses at room temperature; Bottom left: Evolution associated spectra of 3 (5 × 10^{-5} M) in THF with time delays of 0 and 5500 ps obtained upon excitation with 387 nm laser pulses at room temperature; Bottom right: Evolution associated spectra of 4 (5 × 10^{-5} M) in THF with time delays of 0 and 5500 ps obtained upon excitation with 387 nm laser pulses at room temperature.; Please note, that the triplet excited state species are only appearing toward the very end of the fs-TAS time scale. Therefore, the triplet excited state features are not fully resolved. For a better analysis of the triplet excited state features, please see the corresponding ns-TAS (Figure S34).

Table S8. Lifetimes obtained from the fs-TAS measurements of 1 - 4 in THF upon excitation with 387 nm at room temperature determined by global analysis. $\tau_{Sp'}$ and τ_{Sp} are the lifetimes of the unrelaxed and relaxed singlet excited p states, respectively. $\tau_{S\alpha}$ and τ_T are the lifetimes of the starting long-lived singlet and triplet excited states, which are analyzed with ns-TAS measurements (Table S6).

HBC	$\tau_{Sp'}$ [ps]	τ_{Sp} [ps]	$\tau_{S\alpha}$ [ns]	τ_T [ns]
1	0.95	176	>6	>100
2	1.00	238	>6	> 100
3	1.03	208	>6	> 100
4	0.95	215	>6	> 100

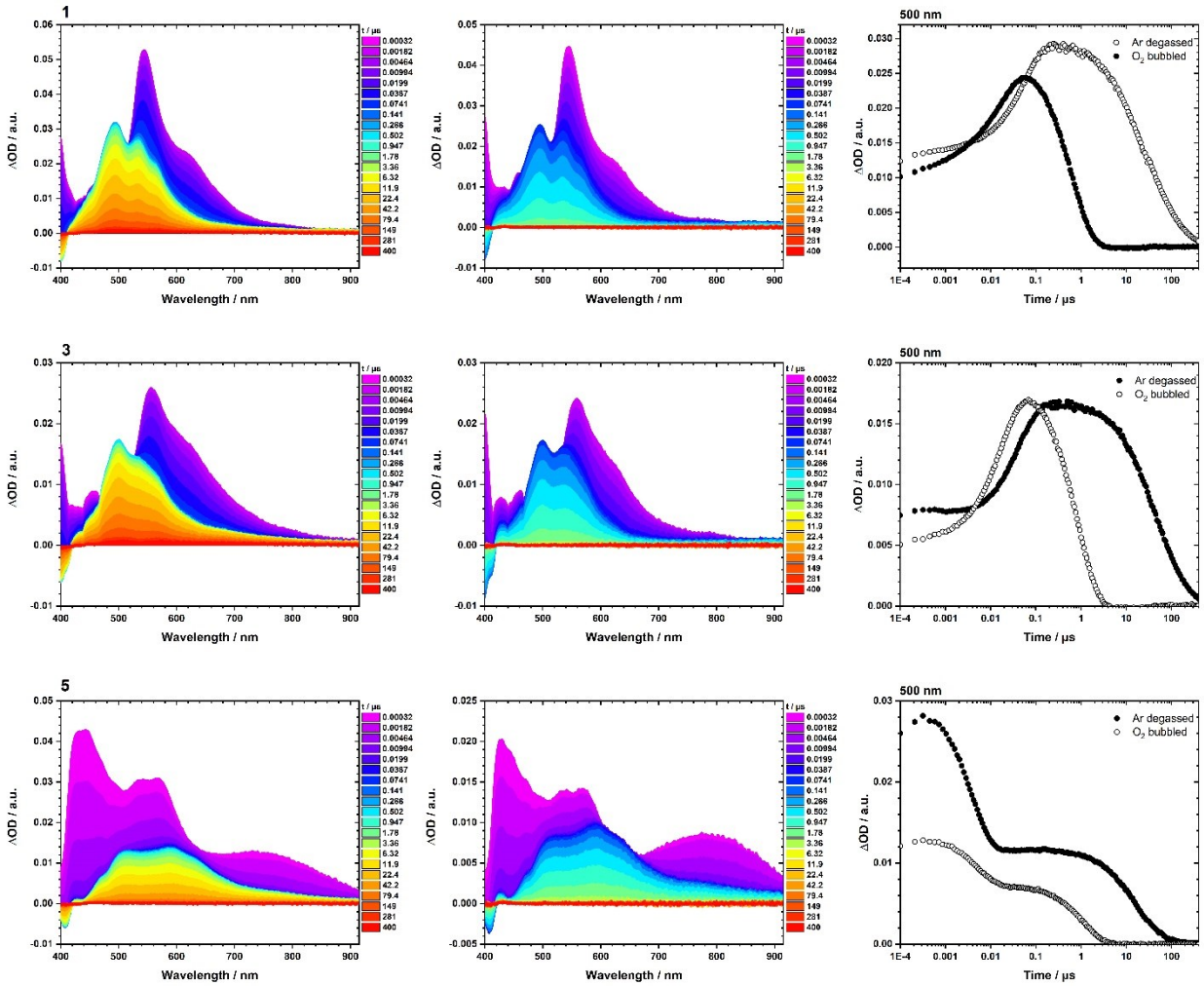

Figure S 34. ns-TAS spectra of **1** (top), **3** (middle) and **5** (down) (5 × 10^{-5} M) in THF after 20 min degassing with argon (**left**) and after 5 min bubbling with dioxygen (**middle**) upon excitation with 387 nm laser pulses at room temperature. On the **right**, the time absorption profiles at 500 nm of the Ar degassed and the oxygen bubbled spectra are compared in order to show the quenching of the triplet in presence of dioxygen.

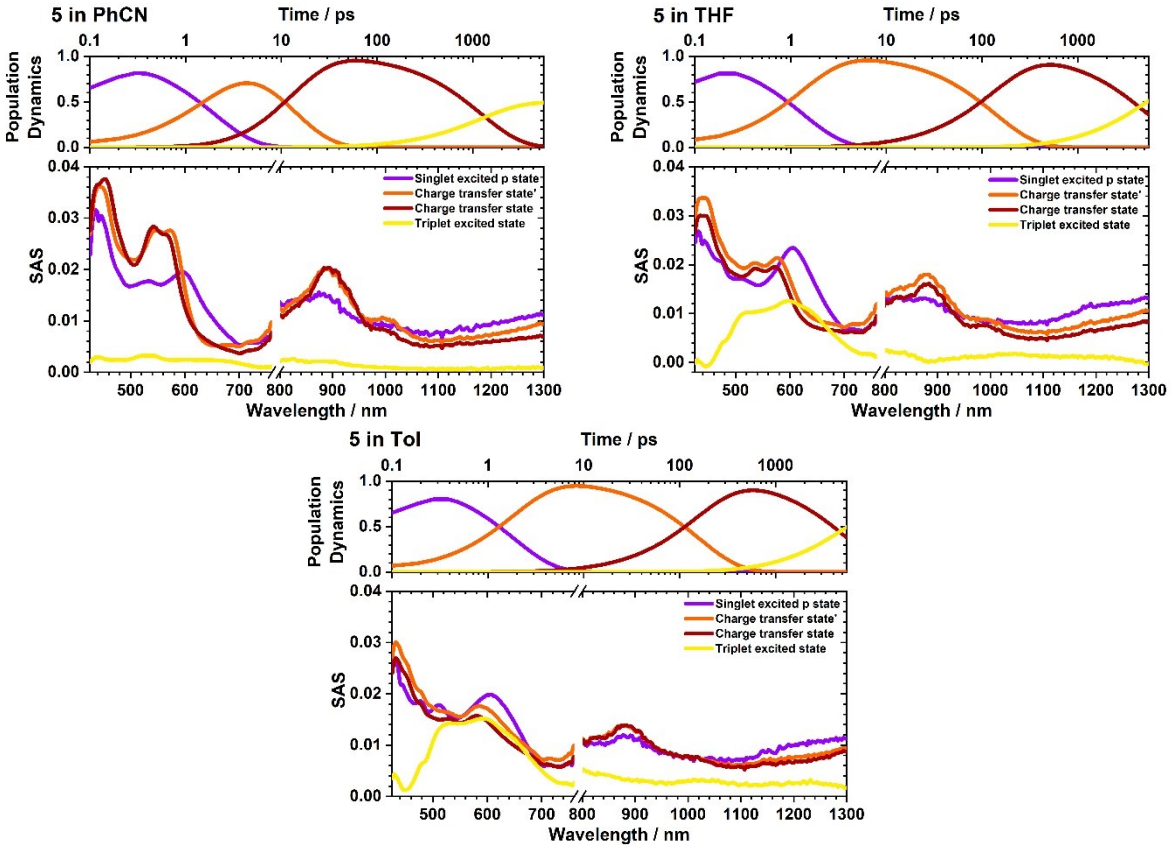

Figure S35. Top left: Species associated spectra of 5 (5×10^{-5} M) received by target analysis in benzonitrile with time delays of 0 and 5500 ps obtained upon excitation with 387 nm laser pulses at room temperature; Top right: Species associated spectra of 5 (5×10^{-5} M) received by target analysis in THF with time delays of 0 and 5500 ps obtained upon excitation with 387 nm laser pulses at room temperature; Bottom: Species associated spectra of 5 (5×10^{-5} M) received by target analysis in toluene with time delays of 0 and 5500 ps obtained upon excitation with 387 nm laser pulses at room temperature.

Table S9. Lifetimes obtained from the TAS measurements of 5 in toluene, THF and benzonitrile upon excitation with 387 nm at room temperature determined by target analysis. τ_{SR} is the lifetime of the structural relaxation of the higher-lying singlet excited state; p state, $\tau_{CT'}$ and τ_{CT} are the lifetimes of the charge transfer states, τ_T are the lifetime of the triplet excited state transients.

-NO_2 (5)	**τ_{SR} [ps]**	**$\tau_{CT'}$ [ps]**	**τ_{CT} [ns]**	**τ_T [µs]**
Toluene	1.9	159	5.5	13.5
THF	2.1	138	5.3	15.0
Benzonitrile	2.0	15.1	1.1	18.0

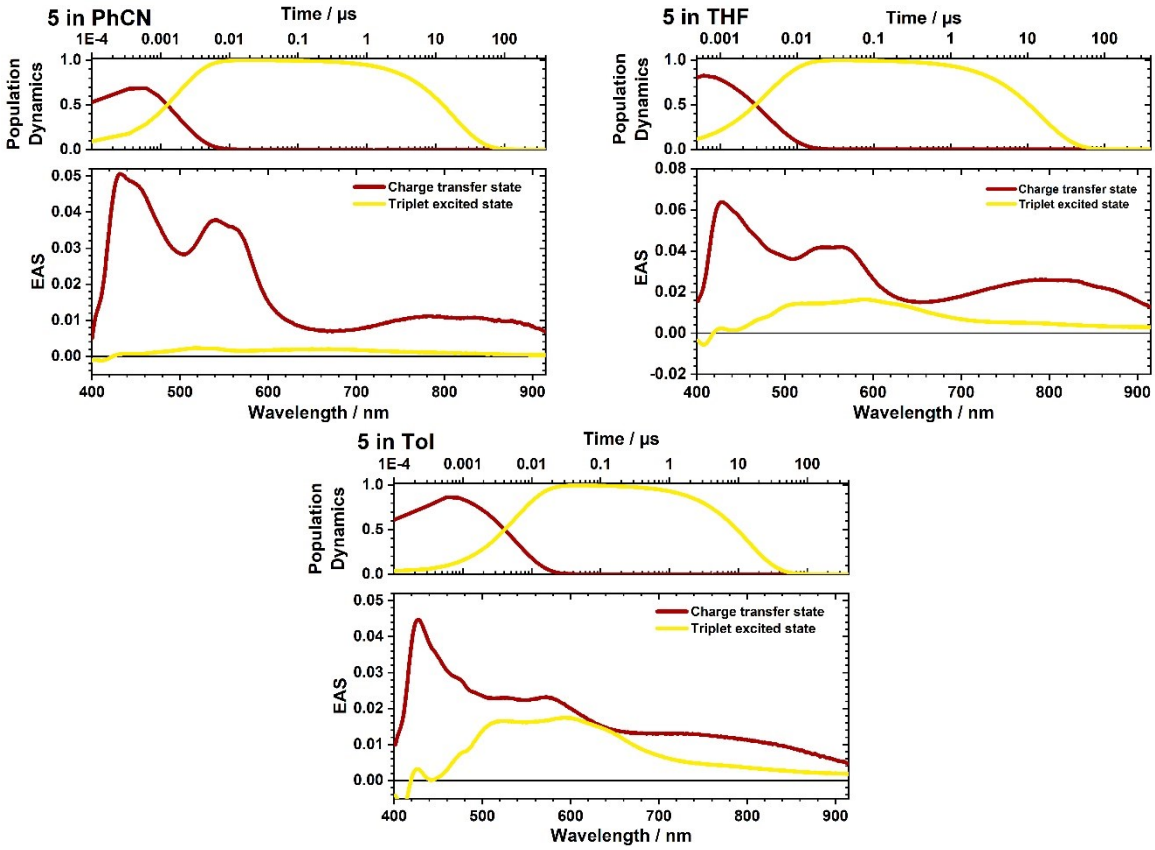

Figure S 36 Top left: Evolution associated spectra of 5 (5 × 10^{-5} M) in benzonitrile in the lower part obtained by global analysis with time delays of 0 and 400 µs obtained upon excitation with 387 nm laser pulses at room temperature and corresponding populations in the upper part; Top right: Evolution associated spectra of 5 (5 × 10^{-5} M) in THF in the lower part obtained by global analysis with time delays of 0 and 400 µs obtained upon excitation with 387 nm laser pulses at room temperature and corresponding populations in the upper part; Bottom: Evolution associated spectra of 5 (5 × 10^{-5} M) in Tol in the lower part obtained by global analysis with time delays of 0 and 400 µs obtained upon excitation with 387 nm laser pulses at room temperature and corresponding populations in the upper part.

Steady-state titrations with TCNE

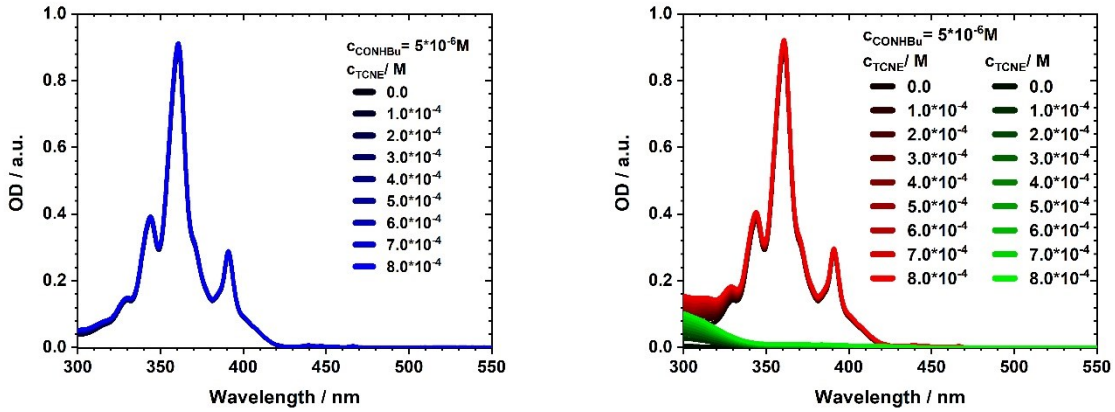

Figure S37. Corrected steady-state absorption spectra (**left**, blue) of functionalized **2** (5 × 10^{-6} M) before and upon addition of TCNE (1 × 10^{-4} − 8 × 10^{-4} M) in THF. The spectra were corrected by subtracting the steady-state absorption spectra of TCNE (**right**, green) with equal concentrations from the steady-state absorption spectra of the titration solution (**right**, red).

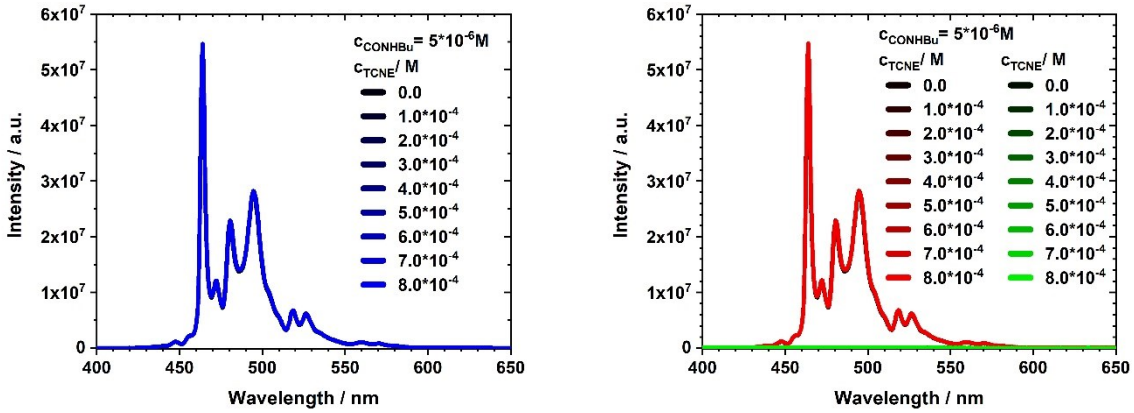

Figure S38. Corrected steady-state fluorescence spectra (**left**, blue) of functionalized **2** (5×10^{-6} M) before and upon addition of TCNE ($1 \times 10^{-4} - 8 \times 10^{-4}$ M) in THF. The spectra were corrected by subtracting the steady-state fluorescence spectra of TCNE (**right**, green) with equal concentrations from the steady-state fluorescence spectra of the titration solution (**right**, red).

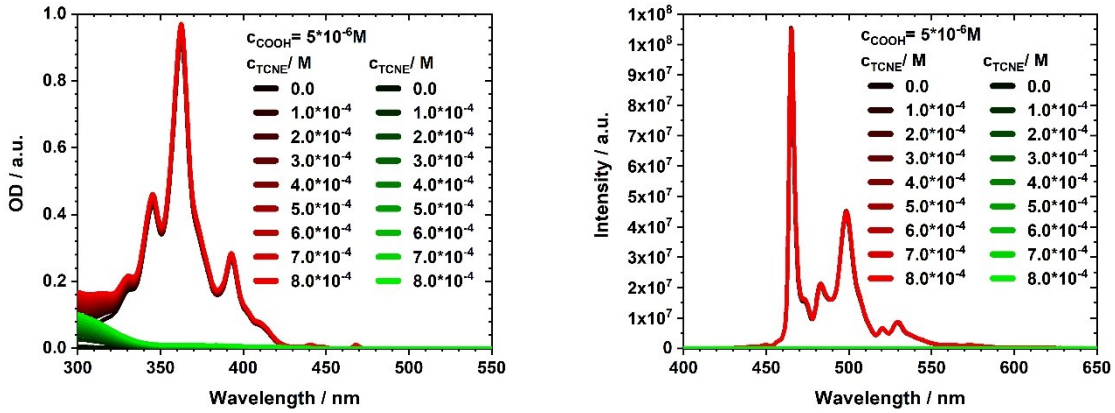

Figure S39. Uncorrected steady-state absorption spectra (**left**, red) and uncorrected steady-state fluorescence spectra (**right**, red) of functionalized **3** (5×10^{-6} M) before and upon addition of TCNE ($1 \times 10^{-4} - 8 \times 10^{-4}$ M) in THF. The corresponding steady-state absorption and fluorescence spectra of TCNE (**left** and **right**, green) with equal concentrations are also shown. The corrected steady-state absorption and fluorescence spectra, in which the TCNE spectra are subtracted from the corresponding titration spectra, are shown in **Figure 9**.

Transient absorption spectroscopy with TCNE

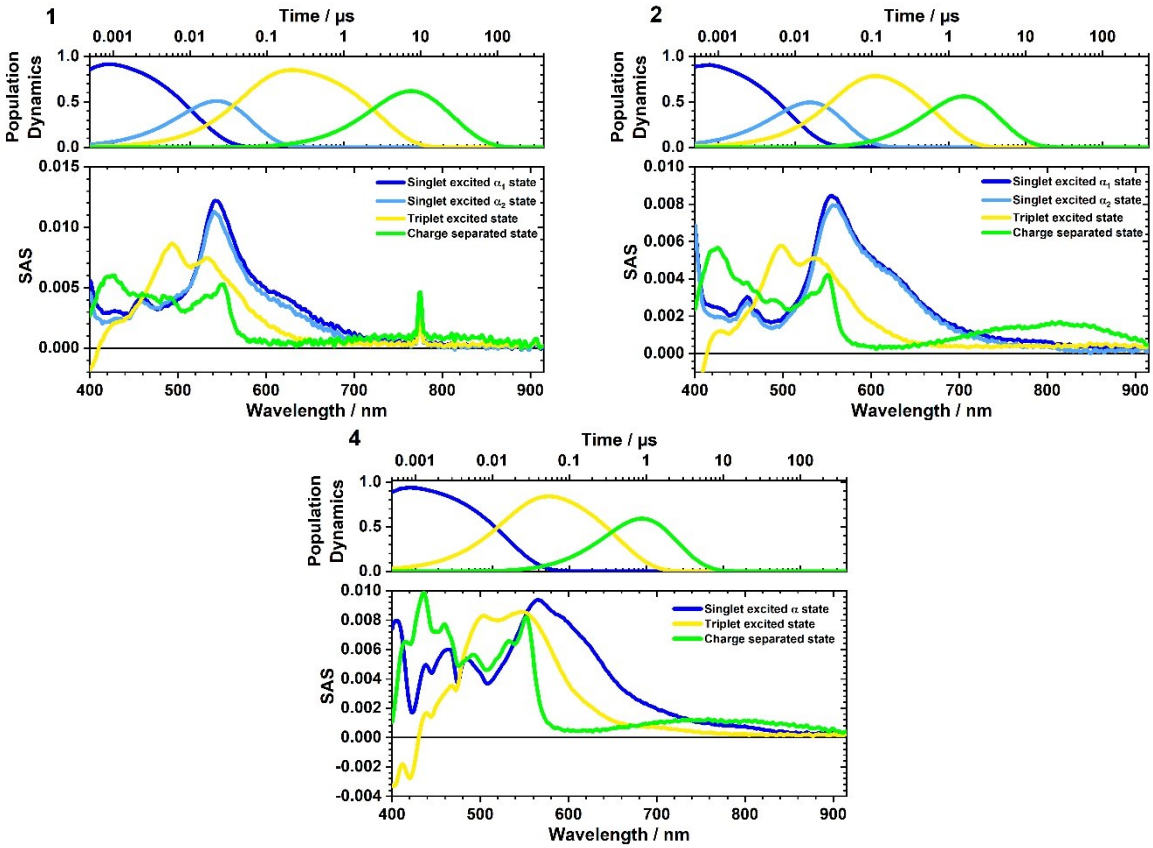

Figure S40. Top left: Species associated spectra and lifetime profile received by target analysis of 1 (5×10^{-5} M) and TCNE (2×10^{-3} M) in THF obtained upon excitation with 387 nm laser pulses at room temperature; Top right: Species associated spectra and lifetime profile received by target analysis of 2 (5×10^{-5} M) and TCNE (3×10^{-3} M) in THF obtained upon excitation with 387 nm laser pulses at room temperature; Bottom: Species associated spectra and lifetime profile received by target analysis of 4 (5×10^{-5} M) and TCNE (2×10^{-3} M) in THF obtained upon excitation with 387 nm laser pulses at room temperature.

Table S10. Transient lifetimes of 1 in THF upon addition of different concentrations of TCNE (2×10^{-3} – 7×10^{-3} M) obtained by target analysis and rate constants of charge separation and recombination.

	TAS of 1		
TCNE	τ_S [ns]	τ_{CS} [ns]	τ_{CR} [µs]
2×10^{-3} M	42.0	2702	22.1
3×10^{-3} M	14.4	56.5	0.674
4×10^{-3} M	12.3	47.1	0.670
5×10^{-3} M	4.31	22.9	0.375
6×10^{-3} M	4.10	21.5	0.371
7×10^{-3} M	3.67	18.2	0.357
Reaction rate of CS		7.9×10^{9} M^{-1} s^{-1}	
Reaction rate of CR		3.5×10^{8} M^{-1} s^{-1}	

Table S11. Transient lifetimes of 2 in THF upon addition of different concentrations of TCNE (3×10^{-3} – 7×10^{-3} M) obtained by target analysis and rate constants of charge separation and recombination.

	TAS of 2		
TCNE	τ_S [ns]	τ_{CS} [ns]	τ_{CR} [µs]
3×10^{-3} M	34.5	1262	7.35
4×10^{-3} M	34.6	629	2.92
5×10^{-3} M	26.9	135	0.818
6×10^{-3} M	22.2	75.6	0.528
7×10^{-3} M	13.8	26.9	0.539
Reaction rate of CS		4.3×10^{9} M^{-1} s^{-1}	
Reaction rate of CR		5.0×10^{8} M^{-1} s^{-1}	

Table S12. Transient lifetimes of 3 in THF upon addition of different concentrations of TCNE (1×10^{-3} – 7×10^{-3} M) obtained by target analysis and rate constants of charge separation and recombination.

	TAS of 3		
TCNE	τ_S [ns]	τ_{CS} [ns]	τ_{CR} [µs]
1 × 10^{-3} M	36.0	26.0 µs	87.1
2 × 10^{-3} M	34.9	743	4.40
3 × 10^{-3} M	19.5	58.1	0.480
4 × 10^{-3} M	21.3	70.3	0.511
5 × 10^{-3} M	12.4	28.5	0.378
6 × 10^{-3} M	11.7	25.2	0.408
7 × 10^{-3} M	6.76	13.9	0.388
Reaction rate of CS		9.5×10^9 M^{-1} s^{-1}	
Reaction rate of CR		3.8×10^8 M^{-1} s^{-1}	

Table S13. Transient lifetimes of 4 in THF upon addition of different concentrations of TCNE (1×10^{-3} – 7×10^{-3} M) obtained by target analysis and rate constants of charge separation and recombination.

	TAS of 4		
TCNE	τ_S [ns]	τ_{CS} [ns]	τ_{CR} [µs]
1×10^{-3} M	15.2	444	1.73
2×10^{-3} M	15.9	456	1.98
3×10^{-3} M	14.7	276	1.57
4×10^{-3} M	11.0	71.7	0.620
5×10^{-3} M	8.81	35.0	0.495
6×10^{-3} M	7.75	28.9	0.434
7×10^{-3} M	6.16	21.1	0.480
Reaction rate of CS		10.6×10^{9} M^{-1} s^{-1}	
Reaction rate of CR		1.7×10^{8} M^{-1} s^{-1}	

Table S14. Transient lifetimes of 5 in THF upon addition of different concentrations of TCNE (1×10^{-3} – 7×10^{-3} M) obtained by target analysis and rate constants of charge separation and recombination.

	TAS of 5		
TCNE	τ_S [ns]	τ_{CS} [ns]	τ_{CR} [µs]
1×10^{-3} M	3.52	1636	6.03
2×10^{-3} M	3.23	510	2.11
3×10^{-3} M	3.36	78.9	0.570
4×10^{-3} M	3.32	66.8	0.512
5×10^{-3} M	3.75	34.3	0.401
6×10^{-3} M	3.47	30.2	0.418
7×10^{-3} M	2.90	24.2	0.318
Reaction rate of CS		7.5×10^{9} M^{-1} s^{-1}	
Reaction rate of CR		3.2×10^{8} M^{-1} s^{-1}	

Steady state absorption spectra of the electrochemically oxidized species

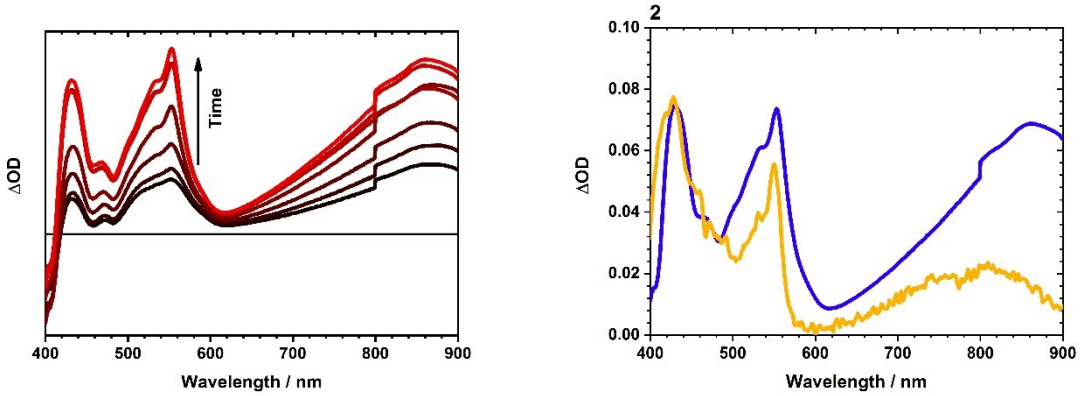

Figure S41. Left: Differential absorption spectra of 2 (c = 10^{-6} M) in dichloromethane (blue) with 0.1 M $TBAPF_6$ upon applying an oxidative potential of 1.0 V. Right: Comparison of the differential transient absorption spectrum of 2 (5 × 10^{-5} M) in the presence of TCNE (5 × 10^{-3} M) in THF at t = 0.77 µs (yellow) and the differential absorption spectrum of 2 (10^{-6} M) in dichloromethane (blue) with 0.1 M $TBAPF_6$ upon applying an oxidative potential of 1.0 V.

References

1 Frisch, M. J.; Trucks, G. W.; Schlegel, H.B.; Scuseria, G. E.; Robb, M. A.; Cheeseman, J. R.; Scalmani, G.; Barone, V.; Mennucci, B.; Petersson, G. A.; Nakatsuji, H.; Caricato, M.; Li, X.; Hratchian, H. P.; Izmaylov, A. F.; Bloino, J.; Zheng, G.; Sonnenberg, J. L.; Hada, M.; Ehara, M.; Toyot,a K.; Fukuda, R.; Hasegawa, J.; Ishida, M.; Nakajima, T.; Honda, Y.; Kitao, O.; Nakai, H.; Vreven, T.; Montgomery Jr., J. A.; Peralta, J. E.; Ogliaro, F.; Bearpark, M.; Heyd, J. J.; Brothers, E.; Kudin, K. N.; Staroverov, V. N.; Kobayashi, R.; Normand, J.; Raghavachari, K.; Rendell, A.; Burant, J. C.; Iyengar, S. S.; Tomasi, J.; Cossi, M.; Rega, N.; Millam, J. M.; Klene, M.; Knox, J. E.; Cross, J. B.; Bakken, V.; Adamo, C.; Jaramillo, J.; Gomperts, R.; Stratmann, R. E.; Yazyev, O.; Austin, A. J.; Cammi, R.; Pomelli, C.; Ochterski, J. W.; Martin, R. L.; Morokuma, K.; Zakrzewski, V. G.; Voth, G. A.; Salvador, P.; Dannenberg, J. J.; Dapprich, S.; Daniels, A. D.; Farkas, O.; Foresman, J. B.; Ortiz, J. V.; Cioslowski, J.; Fox, D. J. Gaussian 09 Revision D.01, Gaussian Inc., Wallingford CT. **2013**

2 C. Adamo, D. Jacquemin, *Chem. Soc. Rev.* **2013**, *42*, 845–856.

3 T. Le Bahers, C. Adamo, I. Ciofini, *J. Chem. Theory Comput.* **2011**, *7*, 2498–2506.

4 W. W. H. Wong, T. Khoury, D. Vak, C. Yan, D. J. Jones, M. J. Crossley, A. B. Holmes, *J. Mater. Chem.* **2010**, *20*, 7005.

5 F. Jäckel, M. D. Watson, K. Müllen, J. P. Rabe, *Phys. Rev. Lett.* **2004**, *92*, 188303.

6 E. Clar, *Polycyclic Hydrocarbons*, **1964**.

7 C. Reichardt, *Chem. Rev.* **1994**, *94*, 2319–2358.

8 P. D. Zoon, A. M. Brouwer, *Photochem. Photobiol. Sci.* **2009**, *8*, 345–353.